



UNIVERSITY OF
CAMBRIDGE

Department of Engineering

Model Rocket Guidance by Canards

Author Name: David Walker

Supervisor: Dr Hugh Hunt

Date: May 2016

I hereby declare that, except where specifically indicated, the work submitted herein is my own original work.

Signed _____ *date* _____

Model Rocket Guidance by Canards: Technical Abstract

David Walker, St John's College, Group C

May 24, 2016

Overview

Model rockets are normally passively stabilised by fins with no means of control. This project is about introducing active control over the 3 axes of rotation: pitch, yaw and roll of a model rocket using technology that is cheap and readily available. Canards (small actuated fins near the top of the rocket) have been chosen to provide the controlling force in the three axes. The project consisted of: airframe construction, inertial measurement unit (IMU) development, wind tunnel testing, linear control theory and flight tests.

Design

The rocket followed standard high powered rocket design practices. It was 100mm in diameter 194cm high and weighed 4.5kg. It contained all the necessary sub systems: motor, drogue chute, deployment computer, main chute, flight computer, canard actuators, camera. It flew on a 2 grain 54mm Cessaroni solid rocket motor reaching an apogee of 800m. The rocket is designed to stay subsonic (below Mach 0.6) and be passively stable. A passively stable rocket has the centre of pressure behind the centre of mass so that a restoring moment is generated when the rocket is not aligned with the airflow.

Construction included fibreglass lay up to reinforce the phenolic body tubes, a selection of water jetted plywood parts, soldering of electronic components, drilling, sawing, sanding and copious epoxy. The IMU uses a Multiwii quadcopter flight computer reprogrammed in the Arduino environment to suit the needs of the project. The 3 axis MEMS (microelectromechanical systems) rate gyroscope is integrated using a direct cosine matrix approach which describes the attitude of the rocket as a rotation matrix.

Testing

The rocket was extensively tested in the Markham wind tunnel to study the aerodynamics of the canards in a controlled environment. Naive assumptions that the canards could

be modelled as simple two dimensional flat plates were thoroughly disproved, leading to a greater understanding of the flow around the rocket and providing quantitative data to inform the control system design. The control system development assumed a linear theory for the rocket based on stability and control derivatives. Transfer functions for the rocket were calculated and used to tune two discrete control loops: roll and pitch.

Whilst rocket flights are very short the preparation leading up to one is lengthy and a significant amount of time was invested in this direction leading to two actual flights, neither with canards in place. Both flights were ultimately unsuccessful due to failure of the recovery system however this meant a number of interesting failures modes had to be understood and solved. Early launches were delayed and ultimately thwarted by smokeless powder, which has been deemed poorly suited to rocket deployment charges. The importance of rigorously testing recovery systems on the ground has been reinforced by the failures. Ultimately serving as a lesson in the challenges of real life engineering and in particular the unforgiving aspects of rocketry. The IMU has been verified on the test flights, as have the deployment section of the flight computer, which was developed from scratch.

Conclusions

- IMU based on direct integration of cheap MEMS gyroscopes verified to have sufficient accuracy for control of model rockets.
- Canards with low aspect ratios are dominated by downwash effects reducing their lift slope but delaying stall.
- Vortices generated by the canards interact with the aft fins in a hard to predict manner, this is more of a problem for roll.
- Coupling between the canards and aft fins makes accurate modelling of the system hard.
- Linear control theory can be applied to rockets to understand and tune feedback loops.
- However the variable velocity during rocket flight severely affects the pitch response making control difficult.
- Dual recovery is harder than it first appears and can hamper development of control systems.
- Smokeless powder is not well suited to use in rocket ejection charges.

Model Rocket Guidance by Canards

Final Report

David WALKER
St John's College
Group C

May 24, 2016

Contents

List of Symbols	2
1 Introduction	3
2 Airframe	4
2.1 Design	4
2.2 Construction	6
3 Inertial Measurement Unit	9
3.1 Theory	9
3.2 Implementation	10
4 Aerodynamics	12
4.1 Experimental Set-up	12
4.2 Results and Discussion	12
5 Control Theory	20
5.1 Linear theory	20
5.2 Roll stabilisation	27
5.3 Pitch and Yaw Autopilot	32
6 Test Launches	40
6.1 January	40
6.2 March	40
7 Conclusions	45
7.1 Future Work	46
7.2 Alternative Paths	47
8 References	48

List of Symbols

ρ	Air density
A	Frontal Area
AR	Aspect ratio
C_D	Drag Coefficient
C_L	Lift Coefficient
C_M	Moment Coefficient
g	Gravitational acceleration
M	Mach number
m	Rocket mass
p	Static pressure
R	Gas constant for air
S	Reference area
T	Temperature
U	Vertical velocity
x	Moment arm

1 Introduction

Out of the various modes of transport rocket flight stands tall as the most expensive, technically complex and most dangerous. All this is necessary for mankind to extend its influence beyond the thin atmosphere around the small planet called Earth into the vastness of space. It is both the enduring challenge and the ability to reach places once thought untouchable that has driven rocket development and inspired this project.

Due to the vast expense of rockets capable of reaching space there has been much work on smaller, model rockets by amateur rocketeers. These are capable of reaching a few kilometres in altitude (although the amateur altitude record stands at an impressive 115km), accelerations easily exceed 10g and velocities are often supersonic.[1] However very little work has been done on active guidance of model rockets. Typically they are passively stabilised by fins with no means of control. However the disadvantages of passive control are firstly the undesirable spinning of the rocket due to slight fin misalignment which reduces the quality of on board video footage. Secondly, passively stable rockets tend to weather cock (turn into the wind) with any deviation from vertical flight reducing the peak altitude of the rocket, motivating the need for pitch and yaw guidance. Furthermore rockets with multiple stages can suffer from directional changes at stage separation events dramatically reducing their altitude. In order to gain control authority over pitch and yaw the roll motion must first be stabilised. This project is about introducing active control over the 3 axes of rotation: pitch, yaw and roll of a model rocket using technology that is cheap and readily available. The project can be split into five main parts: hardware construction, the inertial measurement unit (IMU), wind tunnel testing, control/simulation and flight testing.

This report first describes the design of a suitable airframe to develop the control system around (section 2.1). The subsequent construction followed standard high powered model rocket practices, which are not comprehensively covered in this report but some notable features of the build are detailed in section 2.2. The next important component for the control system is a cheap and accurate inertial measurement unit. Whilst these have become readily available for quadcopters an entirely new firmware was written to meet the needs of rocket control, details of which are in section 3. Having designed and built the airframe using simple expressions for the lift forces that would be generated an assessment of the actual performance was made using the Markham wind tunnel. This confirmed the existence of significant 3D flow effects showing the initial calculations to be far from reality (section 4.2). This data was then used in the control system design detailed in section 5. Two separate

control systems were developed: one for roll and one for pitch or yaw. The final aspect of the project were test launches to produce in flight data (section 6). Two flights have taken place to date, neither have used a canard control system. Both have suffered from failure of the parachute deployment system, albeit in different and interesting ways which are detailed in the section. The launches provided data both from the flight computer sensors and from a small video recorder. These have been used to inform both IMU development and control development.

2 Airframe

2.1 Design

There are a number of ways to control a rocket: aerodynamic surfaces, thrust vectoring, cold gas thrusters and reaction wheels. This project looks at the use of canards which are actuated fins near the top of the rocket; they were chosen based on a number of perceived advantages. Solid rocket motors for model rockets typically have burn durations around 3 seconds making thrust vectoring impractical whereas aerodynamic surfaces can operate over the entire upwards portion of flight.[2] Reaction wheels and cold gas thrusters are heavy due to the requirement for a flywheel and pressure vessel respectively and it is important to keep the weight of the rocket as low as possible.

Locating the control surfaces near the top of the rocket means there is more room for actuators where as the lower section of the rocket is taken up by the motor. However placing aerodynamic surfaces near the top of the rocket reduces the passive stability of the rocket requiring larger aft fins to compensate as explained below. Canards have been extensively used in missiles, which demonstrates the validity of this approach. However whether they can be successfully implemented on a shoe string budget is yet to be done.

The use of canards has driven the airframe design. The diameter of the rocket was chosen to be 100mm in order to accommodate four standard size servos. The height of the rocket is such as to accommodate all the necessary sub systems: motor, drogue chute, deployment computer, main chute, flight computer, canard actuators, camera. This resulted in an airframe 194cm high and weighing 4.5kg. An upwards flight time of 15 seconds can be achieved using a motor with a J impulse rating (640—1,280Ns). 54mm Cesaroni solid rocket motors are readily available at rocket launch events so provide the most convenient means of propul-

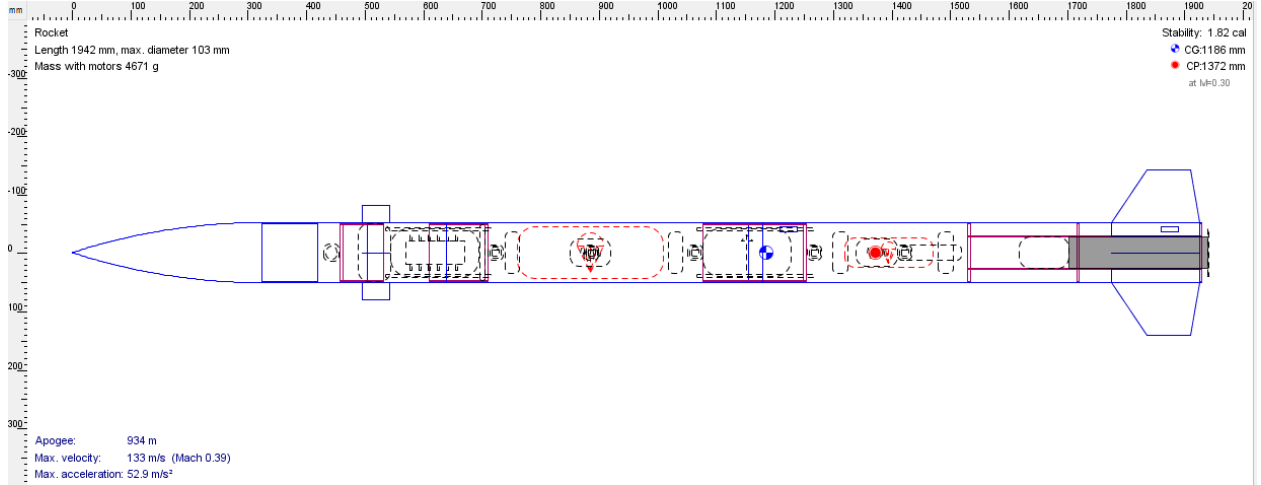


Figure 1: The OpenRocket model is used to find the centre of mass and centre of pressure of an airframe. It also simulates flights to provide estimates for maximum velocities and altitudes.

sion. The rocket design has been informed by rocket specific design software (OpenRocket, figure 1) to ensure the rocket stays subsonic (below Mach 0.6) and is passively stable. A passively stable rocket has the centre of pressure behind the centre of mass so that a restoring moment is generated when the rocket is not aligned with the airflow. The stability margin is the distance between the centre of pressure and the centre of mass divided by the body diameter. A rule of thumb for model rockets is to have a stability margin between 1 and 2. Too low and the rocket may go unstable, too high results in increased drag and weight from excessively large fins and increased susceptibility to weather cocking. Once the centre of mass is known this design rule sizes the fins.[3]

Dual deployment is when a small parachute (the drogue parachute) is released at apogee (maximum altitude), followed by a larger chute (the main) at a lower altitude. This reduces the drift of the rocket during descent whilst still achieving a soft landing (preventing damage to the rocket). The drogue chute is 60cm in diameter resulting in a descent rate of 13m/s whilst the main has a diameter of 210cm for a descent rate of 4m/s. These are found using the below formula which sets the drag force equal to the weight.

$$U_{descent} = \sqrt{\frac{2mg}{C_D \rho A}} \quad (1)$$



(a) Motor tube with centreing rings (left) and fins (right) prior to assembly.



(b) A view from the rear of the rocket showing the through wall mounting of the fins, a third centreing ring is yet to be fixed to close this end.

Figure 2

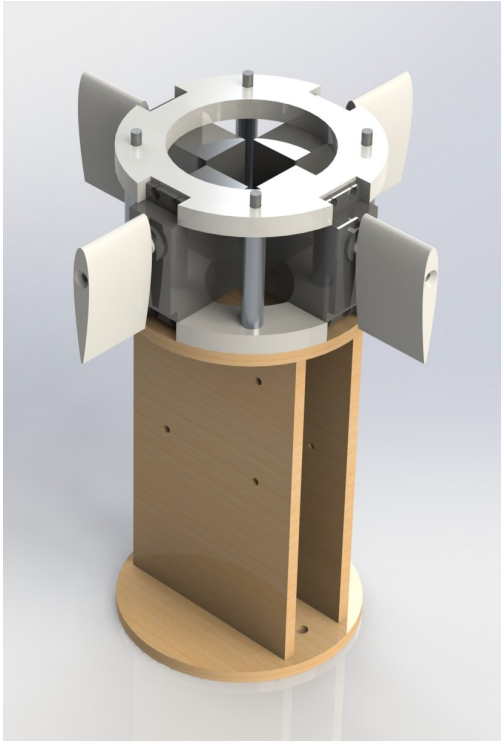
2.2 Construction

Fundamentally rockets are a set of tubes with a suitable internal structure to support all the internal systems. The challenge is in designing and manufacturing the airframe to be strong enough whilst as light as possible. Composites provide high strength for low weight which is why the phenolic body tubes (a type of cardboard) were coated with fibreglass and the aft fins were made from 3mm G10 fibreglass sheet. The motor tube (58mm in diameter) is smaller than the body tube (100mm) so is mounted inside the body tube using 5mm plywood centring rings, cut on a water jet. This means the fins can be mounted through the wall of the body tube resulting in a much stronger construction compared with attaching the fins directly to the outer tube. These are shown prior to assembly in figure 2a and after assembling in figure 2b.

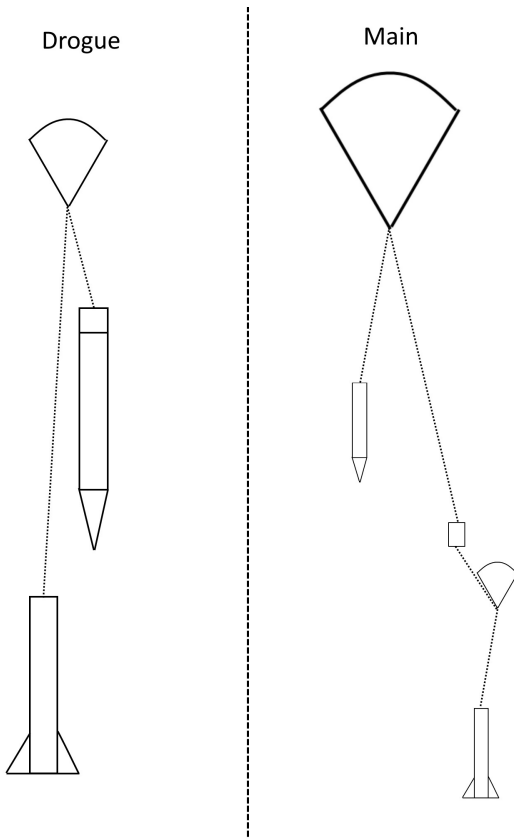
To control the rocket four servo actuated canards are used, with a chord of 50mm, span of 30mm and a NACA 0015 profile. They were 3D printed and mounted directly to the servo output shaft, figure 3a. A long M3 steel screw passes through the canards to hold them firmly onto the servo. The driving torque is transferred through a modified servo horn at the quarter chord point where the lift force will act, this reduces the torque required from

the servo. The servos need to be strong enough to take the maximum lift, drag and pitching moments from the canards. The maximum pitching moment during normal flight should be well below 9Ncm, with a worst possible case of the canard perpendicular to the flow of 45Ncm. The servos also need to accurately position the canards. Originally the canards were designed to operate between $\pm 10^\circ$ limited by aerodynamic stall which would require the canard angle to be controlled to the nearest 1° . On investigation the Hitec HS-5485 servos used do not produce their rated torque until deflection from the desired angle exceeds about 5° . This is explained by the simple proportional feedback controller used in the servos. However due to 3D flow the operating range of the canards is $\pm 30^\circ$ relaxing the constraints on the servos.

The parachutes are deployed by explosive charges that pressurise the parachute compartment causing nylon shear pins to break and the rocket to separate. The charges are ignited with an electric match activated by a commercial Perfectflite deployment computer. The built in motor ejection charge acts as a back up for drogue deployment and the control computer acts as a back up for the main. A section of flame proof Kevlar cord is tied to eye nuts in the airframe followed by more elastic 5mm braided nylon cord to reduce the shock load at deployment. Flame proof Nomex sheets protect the parachutes from the explosive charges and swivels prevents the parachutes from tangling. The lengths of the nylon cord are such that the different sections do not bash into each other after separation, see figure 3b.



(a) Solidworks model showing the four servos and canards supported by two nylon discs, below is the plywood flight computer sledge which supports the flight computer and its subsystems.



(b) Layout after drogue chute deployment (left) showing that the two halves of the rocket are not in contact. Right shows the layout after main deployment.

Figure 3

3 Inertial Measurement Unit

3.1 Theory

The IMU uses sensors to output the attitude of the rocket for use in the control system. In order to compute the attitude the rate gyroscopes are integrated using an approach based on the direct cosine matrix which accounts for the non-commutative nature of rotations.[4] In equation 2 the rotation matrix $\mathbf{R}(t)$ is multiplied by the matrix built from small rotations in each axis $d\theta$ to provide an updated matrix $\mathbf{R}(t + dt)$ which replaces $\mathbf{R}(t)$ on the next loop. Due to accumulation of errors the matrix must be renormalized after each update. A system based solely on gyroscopes suffers from drift due to errors in the magnitude of the gyroscope readings, the limited sample rate and the discrete integration. The challenge is to maintain an accurate attitude measurement for the duration of the controlled flight (about 20s) using cheap and relatively inaccurate MEMS (microelectromechanical systems) gyros.

$$\mathbf{R}(t + dt) = \mathbf{R}(t) \begin{bmatrix} 1 & -d\theta_z & d\theta_z \\ d\theta_z & 1 & -d\theta_x \\ d\theta_y & d\theta_x & 1 \end{bmatrix} \quad (2)$$

It is common to correct for drift using the gravity and magnetic reference vectors, obtained using an accelerometer and magnetometer respectively. However the gravity vector can not be directly measured during rocket flight due to the constantly changing acceleration of the rocket. However over the short time of the flight the gyros should provide sufficient accuracy. This has been verified to be the case through test flights, conducted without active control. Position can be measured by a GPS and a barometer. The barometer measures the static air pressure which decreases as the rocket ascends. The altitude can be approximated over short distances by assuming a constant density, equation 3, this saves on the limited computation time. Assuming a near vertical trajectory the velocity can be estimated from the barometer.

$$Altitude \approx \frac{2(p_{ground} - p)}{p_{ground} - p} \frac{RT}{g} \quad (3)$$

The flight computer needs to reliably detect launch and apogee to serve as a parachute deployment computer. The event detection criteria are listed in table 1.

Event	Criteria
Launch	Acceleration $> 4g$
Confirmed launch	Altitude gain since launch exceeds 50m within 3s
Apogee	Vertical velocity < 0
Main deployment	Altitude $< 250m$

Table 1: Conditions used by the flight computer to detect the key events during the rocket's flight.



Figure 4: The Multiwii flight board contains a microprocessor, accelerometers, gyroscopes, magnetometers and a barometer yet is only 50mm by 50mm.

3.2 Implementation

A Multiwii quadcopter flight computer (figure 4) has been re-purposed using custom firmware written in the Arduino environment. This board contains an MPU6050 combined accelerometer and gyroscope and a MS561101BA barometer. The target sample rate is 200Hz. A separate serial data logger (Sparkfun OpenLog) is used to record the sensor outputs onto a SD card so that flights can be analysed. A separate circuit based on a N channel enhancement mosfet and a capacitor allows this computer to fire a deployment charge if required (figure 5). The computer was first test flown in a non flight critical role which proved valuable as several bugs were discovered and have since been fixed.

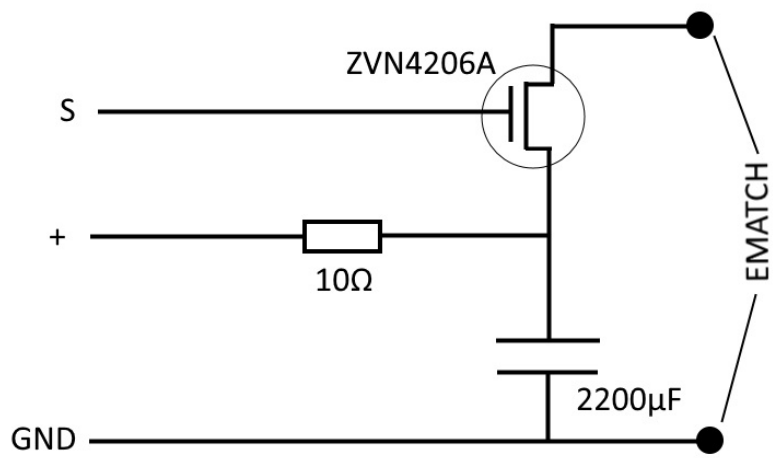


Figure 5: Schematic of the circuit used to fire an e-match for parachute deployment by the Multiwii flight computer.

4 Aerodynamics

During the initial design the forces due to the canards were estimated using 2D flat plate theory, in order to verify this analysis wind tunnel tests on the full scale rocket were conducted.

4.1 Experimental Set-up

Due to the rocket's size the only wind tunnel suitable was the Markham in the engineering department with a test section size of 1.7m x 1.1m x 2.5m.[5] The rocket was mounted on a sting balance, this measures forces and moments in 3 orthogonal directions which are output to a computer system. This required a suitable adaptor to be machined out of aluminium to fit inside the motor mounting tube and onto the sting balance. The balance is also electrically actuated allowing a series of measurements at different angles to be quickly taken. Whilst the expected loads fell well within the rated capacity of the balance, there were initial concerns over the stiffness of the mounting which could lead to oscillations and catastrophic failure of the load cells. Fortunately the system remained stable and tests were conducted at 5mbar dynamic pressure (about 30m/s).

4.2 Results and Discussion

The rocket must operate over a wide range of velocities up to 200m/s. The flow is at sufficiently high Reynold's number for the boundary layers to be turbulent and therefore the flow pattern is independent of Reynolds number. This means the lift and drag coefficients measured in the tunnel at 30m/s will be the same as those experienced at higher velocities. This was verified by running the wind tunnel at two different speeds and checking the lift coefficients were the same.

However for speeds above Mach 0.3 (100 m/s) compressibility needs to be taken into account which can be achieved using Glauert's compressibility factor (equation 4), where C_{L0} is the lift coefficient in incompressible flow. The rocket is not intended to fly in the transonic or supersonic regimes where the flow structure changes dramatically.

$$C_L = \frac{C_{L0}}{\sqrt{1 - M^2}} \quad (4)$$



Figure 6: The rocket mounted on the sting balance in the Markham wind tunnel, the sting balance measures forces and moments in 3 axes and provides automated pitch sweep. The motor tube provided a convenient mounting point.

Firstly the stability of the rocket with the canards aligned with the body of the rocket was tested. This was done by measuring the lift force and pitching moment over a range of incidences to find the centre of lift. Expressing this as a stability margin (the distance between the CP and CG normalised by the body diameter) results in figure 7. The margin is seen to always be greater than 2.5 showing that the OpenRocket value of 1.8 was conservative. The large values at small incidences are probably due to the small absolute readings resulting in a large uncertainty.

$$\text{Centre of lift} = \frac{\text{Pitching moment}}{\text{Lift}} \quad (5)$$

The four canards can be set independently, to achieve a pitching moment two canards are angled symmetrically, similarly a yaw moment is generated by angling the two canards in the perpendicular plane. While a roll moment is generated by angling all four canards anti-symmetrically. Pitch, yaw and roll can be achieved by superimposing the three commands.

Canard pitch control was investigated by setting different canard pitch commands and measuring the resulting pitching moment (figure 8). This was significantly lower than expected,

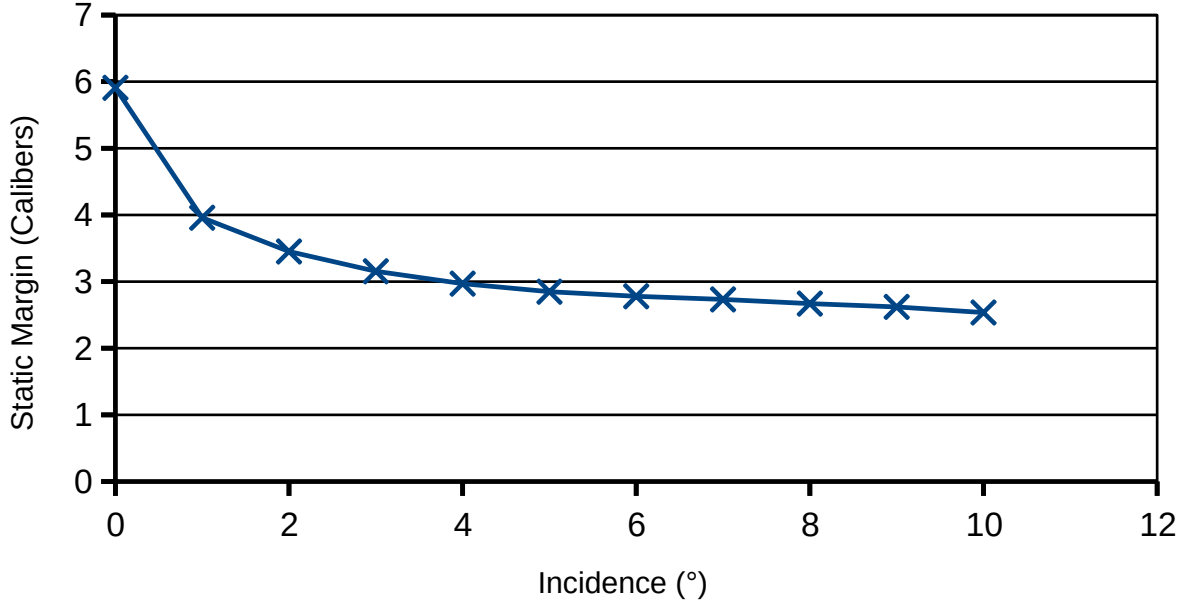


Figure 7: Static margin against angle of attack, showing an asymptote around 2.5 which is acceptable. This is a measure of the static stability of the rocket.

figure 9 has been produced by back calculating the canard lift coefficient and comparing this to the 2D value. The measured values are about 20% of 2D values. This can be explained by the low aspect ratio of the canards ($AR=0.6$). A vortex forms at the tip of a wing because the upper surface is at low pressure while the lower surface is at high pressure. This produces downwash on the wing lowering the local angle of attack. This was confirmed by the stall angle of the canards which was well above 30° while a 2D profile would stall around 12° . A correction factor from the literature is written below, however this does not match the measurements.[6] This is likely due to the exceedingly low aspect ratio of the canards, comparing with data for $AR=0.5$ in figure 10 the values are in agreement. The same back calculation has been done using the data from canard roll commands, these are seen to be much lower again, requiring a further explanation.

$$AR = \frac{span}{chord} \quad (6)$$

$$C_L = \frac{C_{L0}}{1 + \frac{C_{L0}}{\pi AR}} \quad (7)$$

To explain the low roll moments requires consideration of the interaction between the canards' downwash and the aft fins. Figure 11 shows how the downwash from the canards

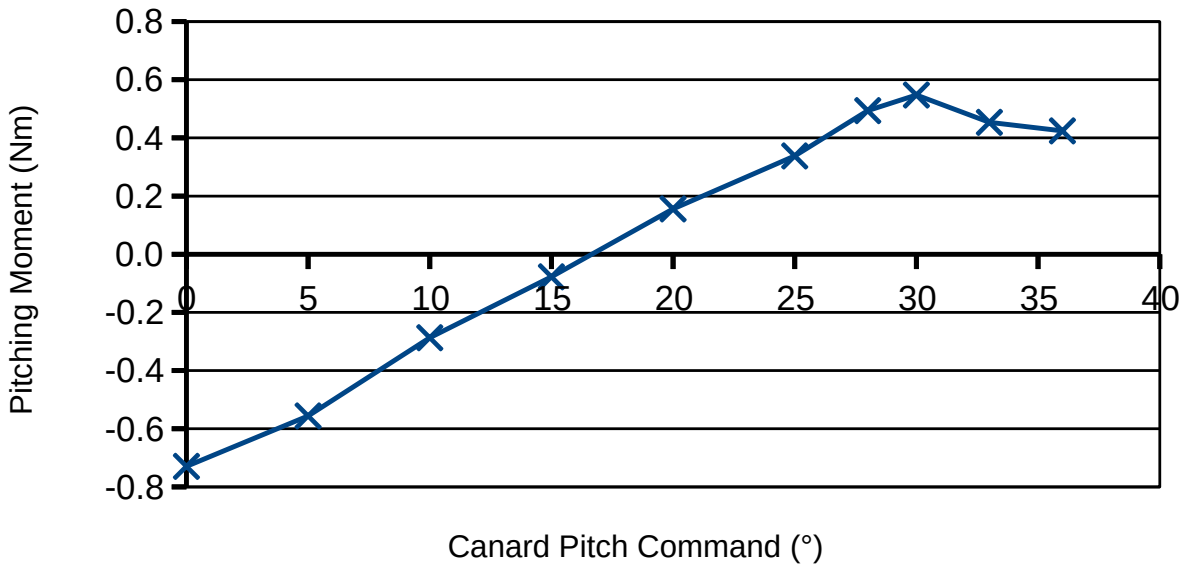


Figure 8: Pitching moment against canard pitch command. The response is linear up to around 30° where the canards stall. The moment starts negative due to the orientation of the rocket which was not exactly parallel to the flow.

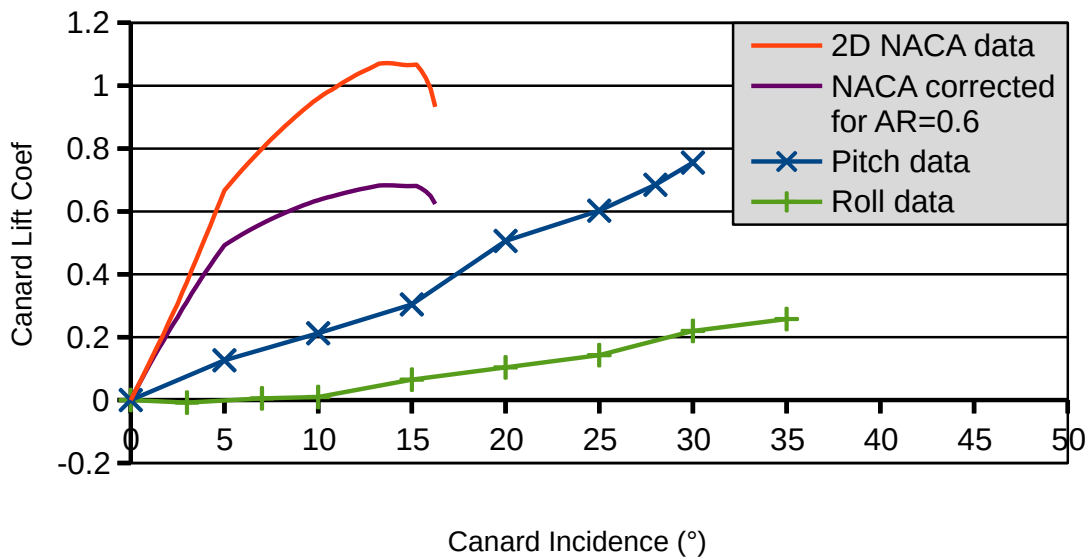


Figure 9: Comparison between the 2D lift coefficient of the canards with back calculated values from the pitch and roll moment data showing the measured values to be much lower than expected.

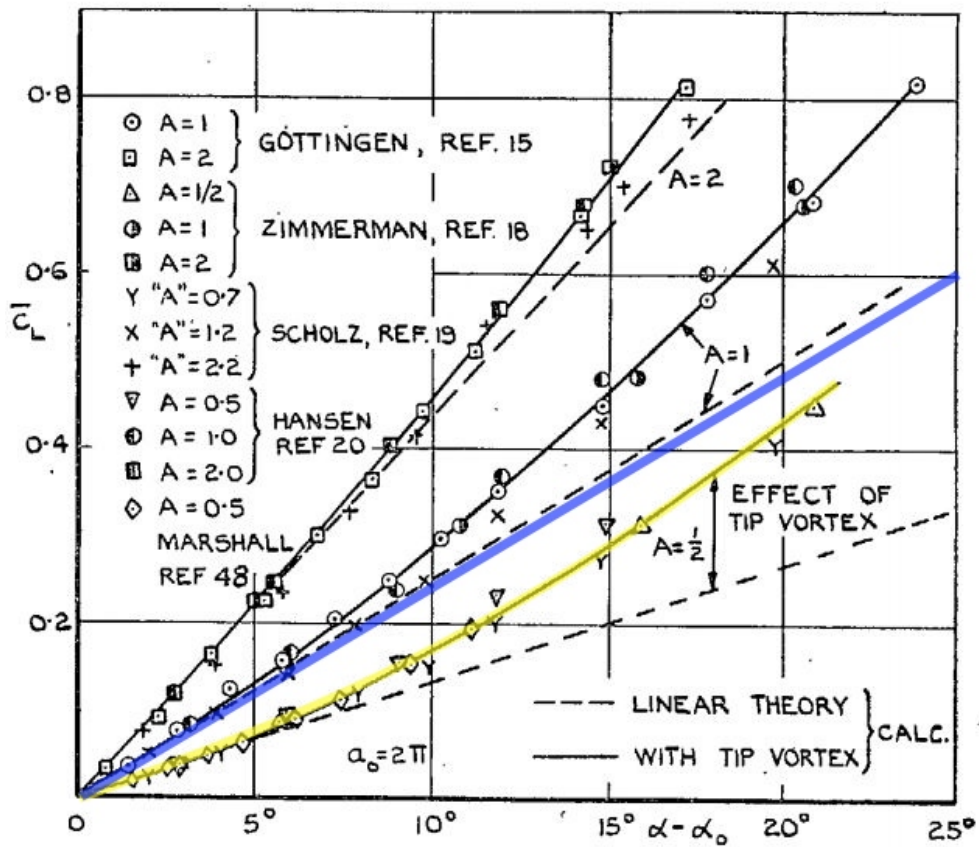


Figure 10: The figure shows experimental data for wings at different aspect ratios along with theoretical predictions (straight lines) from a report by D. Kückemann. The blue line corresponds to the canard lift coefficients found from the pitch data. The yellow line highlights the results from the closest aspect ratio (0.5 compared with 0.6 for the canards). [7]

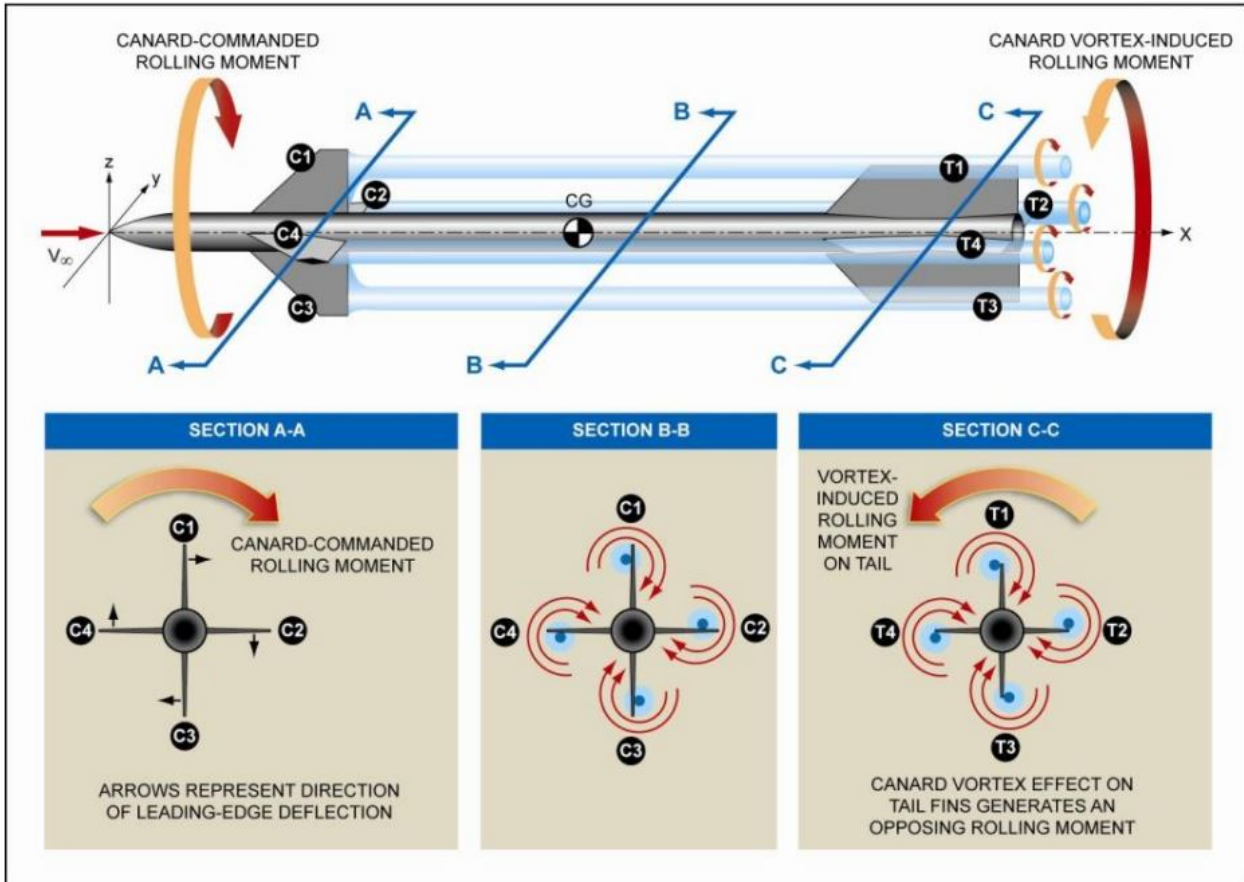


Figure 11: Diagram showing how the vortices generated by canards from a roll command create an opposing rolling moment at the aft fins. From a report by Melissa McDaniel, Christine Evans and Dan Lesieutre.[8]

results in an opposing roll moment generated by the aft fins. A similar phenomena occurs for pitch but the effect is complementary (figure 12). Furthermore there are likely to be dynamic effects due to the lag between the vortex generation at the canard and when it interacts with the aft fins. Offsetting the canards by 45° to the fins whilst certainly changing the characteristics, would only move the problem to a different combination of pitch, yaw and roll. It would not make the canards' behaviour any easier to predict.

The roll control of the canards was assessed by applying a range of canard roll commands and performing a pitch sweep. The roll moment generated varied considerably as the rocket incidence increased. For small canard angles the roll moment actually reversed. This was due to the vortices from the canards intersecting with the aft fins as described above.

The addition of a yaw command to the canards is also shown to dramatically effect the roll moment generated especially at higher incidences. Therefore the aerodynamics are not linear

and cannot be superimposed as accurately as originally hoped.

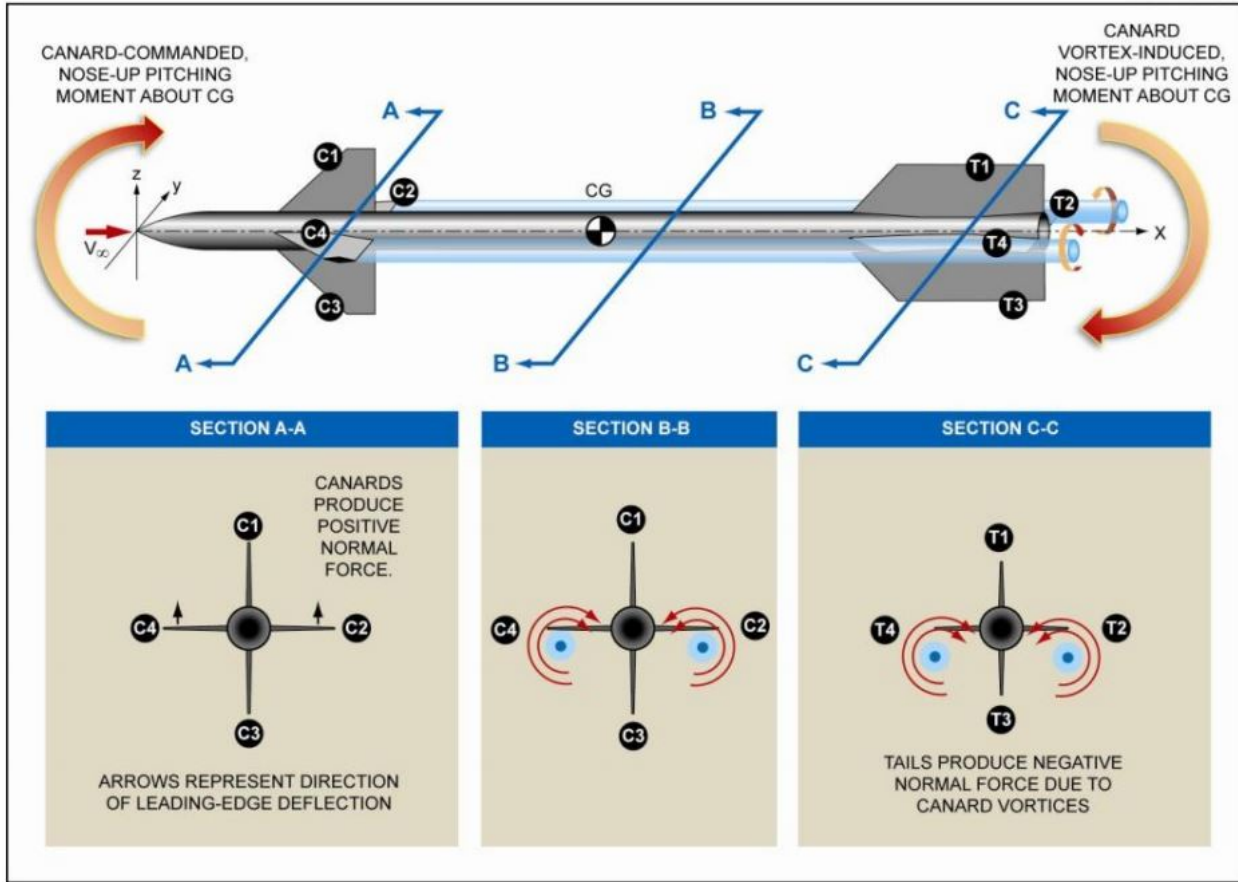


Figure 12: Diagram showing how the vortices generated by canards from a pitch command produce a complimentary pitching moment at the aft fins. From a report by Melissa McDaniel, Christine Evans and Dan Lesieurte.[8]

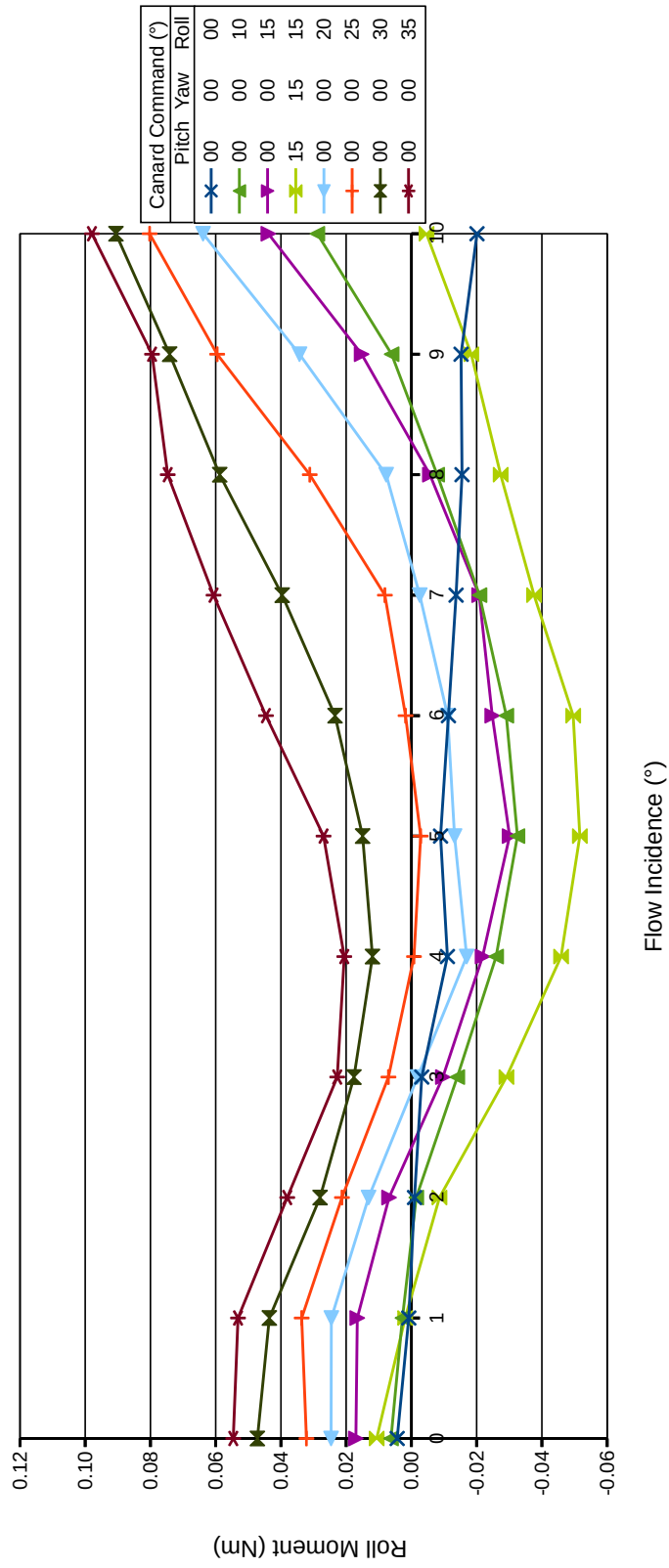


Figure 13: The chart shows the rolling moment generated by a range of canard commands (detailed in the legend) over a range of flow incidences. The roll moment is strongly influenced by the flow incidence, as incidences increase up to 5° the moment is reduced; for a roll command less than 25° the moment is actually reversed. The pale green line shows a combined command of pitch, yaw and roll, it is clear that this has not produced a rolling moment equivalent to a pure roll command as would be expected by superposition.

5 Control Theory

The approach taken to designing the control system was to develop a linear model of rocket then use root locus plots to find appropriate feedback constants for roll stabilisation and a pitch or yaw autopilot.

5.1 Linear theory

In order to describe the rocket by linear differential equations requires the motion to be characterised as small perturbations about an equilibrium state. Where the equilibrium state is straight flight with zero roll rate, at constant velocity. The assumption of constant velocity is obviously not correct however by running the model at different velocities its effect can be investigated. During this section the following notation will be used.

Notation			
Pitch	θ rad	Lateral Force 1	Y N
Pitch rate	q rads $^{-1}$	Pitch Moment	M Nm
Yaw	ψ rad	Lateral Force 2	Z N
Yaw rate	r rads $^{-1}$	Yaw Moment	N Nm
Roll	ϕ rad	Axial Force	X N
Roll rate	p rads $^{-1}$	Roll Moment	L Nm
Surge	u ms $^{-1}$	Pitch Command	dq rad
Sideslip	v ms $^{-1}$	Yaw Command	dr rad
Heave	w ms $^{-1}$	Roll Command	dp rad

The aerodynamic forces resulting from unsteady motion will depend on the current and past state of the rocket, however the forces will be dominated by the current linear and angular velocities. Making this assumption allows each aerodynamic force and moment to be expressed in terms of velocities and corresponding stability derivatives or a control command and corresponding control derivative. For example,

$$M(t) = M_w w(t) + M_q q(t) + M_{dq} dq(t) \quad (8)$$

The assumption that all the aerodynamic forces behave in a linear fashion is not well supported by the wind tunnel data which showed that combining pitch, yaw and roll canard

View from rear

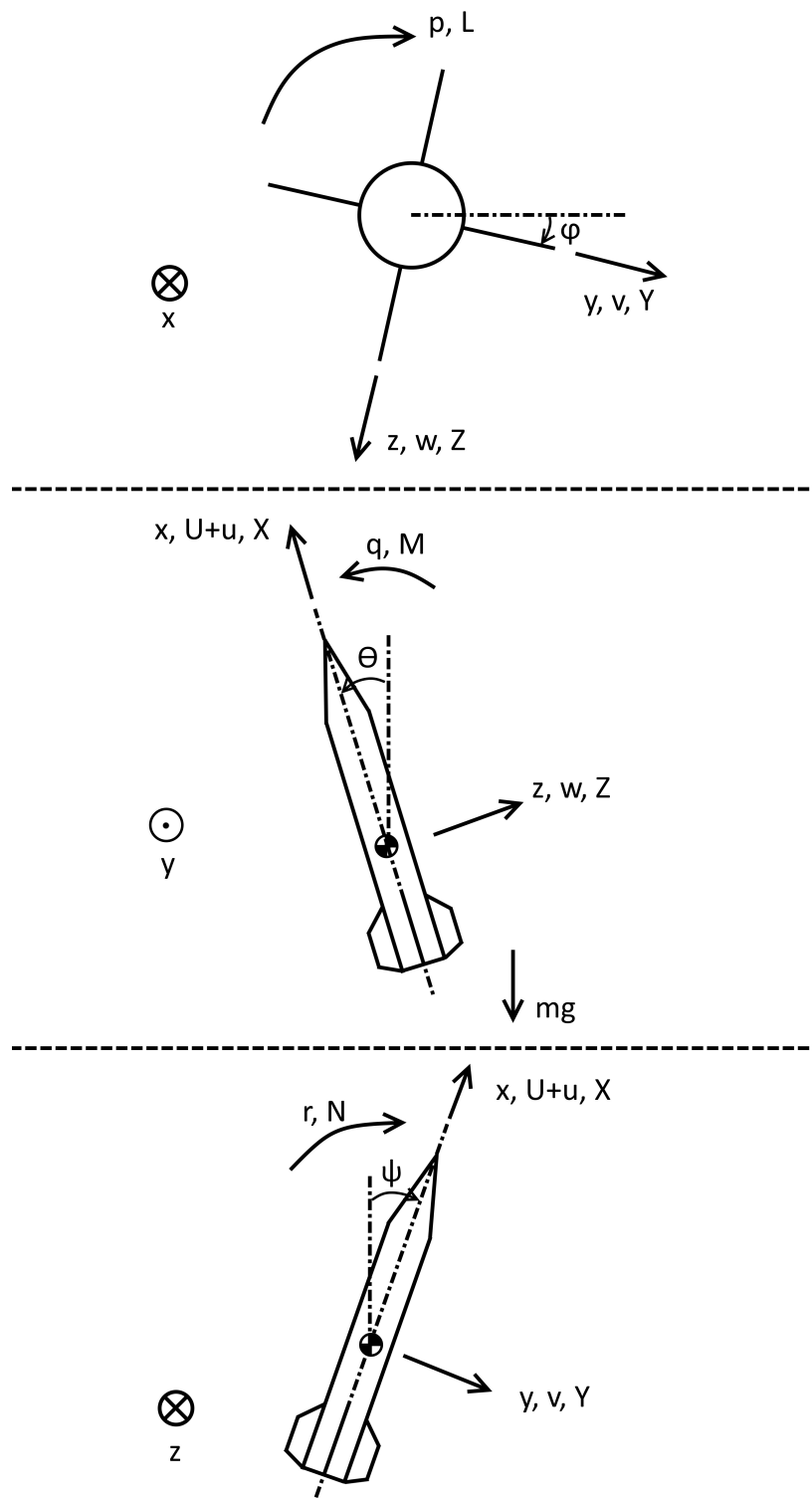


Figure 14: Three orthogonal views of a rocket showing the direction of linear and angular velocities, forces and moments, where x,y,z are the three axes.

commands did not produce the forces expected by superposition (figure 13). However approximating the system as linear allows the analysis to proceed simply and hopefully with sufficient accuracy to provide initial values for the control constants which can then be adjusted based on actual flight data.

The stability and control derivatives have been found from the wind tunnel data, figures 15 to 20 provide the data in non-dimensional form where the respective quantities take their normal form as defined below.

$$C_L = \frac{\text{Lift}}{0.5\rho U^2 S} \quad C_D = \frac{\text{Drag}}{0.5\rho U^2 S} \quad C_M = \frac{\text{Moment}}{0.5\rho U^2 S x} \quad (9)$$

The slope of the line of best fit in each case is used to find the derivative. For example to find Z_w consider the force $Z_w w$; the component of Z due to w, the heave velocity.

$$Z_w w = -C_L 0.5\rho U^2 S \quad (10)$$

From figure 19, accounting for the conversion from degrees to radians:

$$C_L = \theta \cdot 0.013 \cdot 180/\pi \quad (11)$$

Noting that $\theta = w/U$ gives $Z_w = -3.7 \times 10^{-3}/\rho U$

A problem arises for the angular velocity derivatives such as Z_q as these could not be measured in the wind tunnel. The most significant aerodynamic force due to a rotation will be generated by the aft fins, due to their relatively large size and distance from the CG. The tail fins are 660mm behind the CG, the incidence of the flow onto the fins is therefore $0.66q/U$. The aft fins were observed to stall between 8° and 9° suggesting that the fins are well modelled by a 2D flat plate. The area of each fin (2 in each plane) is 0.01 m^2 , the lift coefficient for a flat plate is simply 2π times the incidence, giving:

$$Z_q = 0.02\pi \cdot 0.66\rho U \quad (12)$$

M_q is simply given by $0.66Z_q$. For L_p a similar argument can be used except the variation in distance from the central axis to the fin varies significantly across the span. Both the relative angle of attack and the moment arm vary requiring an integral approach.

The remaining derivatives can be found by symmetry between the pitch and yaw planes. The body properties have been extracted from the Solidworks model.

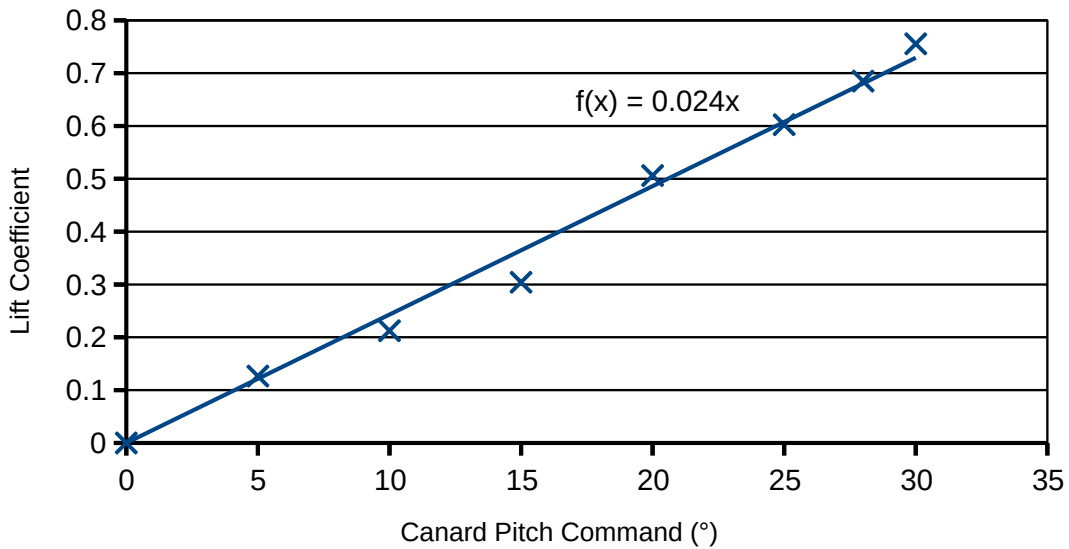


Figure 15: Lift coefficient against canard pitch command, the gradient is used to calculate the control derivative Z_{dq} using reference area, $S = 3 \times 10^{-3} \text{ m}^2$. The behaviour is clearly linear as assumed by the model.

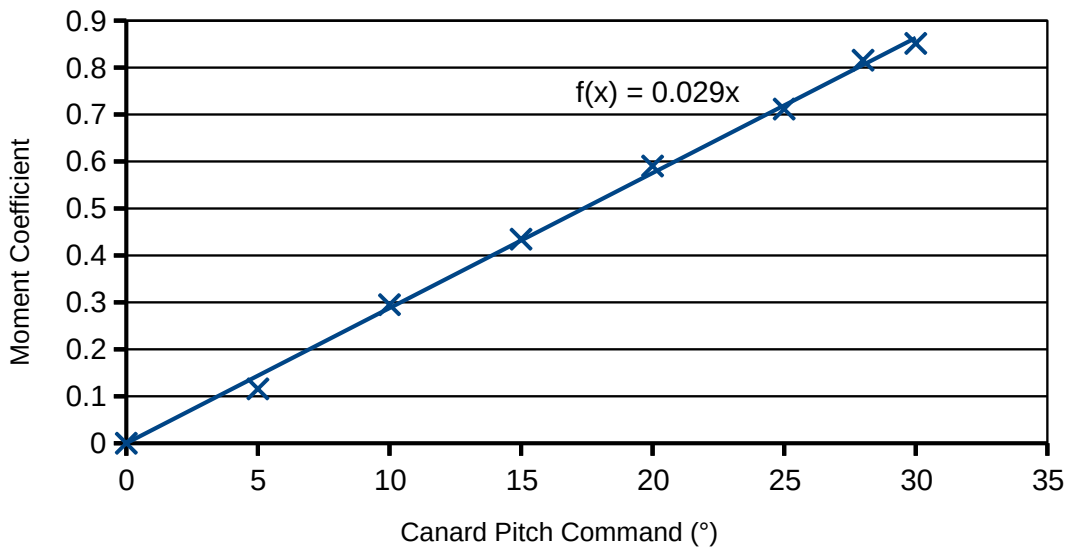


Figure 16: Pitching moment coefficient against canard pitch command, the gradient is used to calculate the control derivative M_{dq} using reference area, $S = 3 \times 10^{-3} \text{ m}^2$ and reference length, $x = 1 \text{ m}$. The behaviour is clearly linear as assumed by the model.

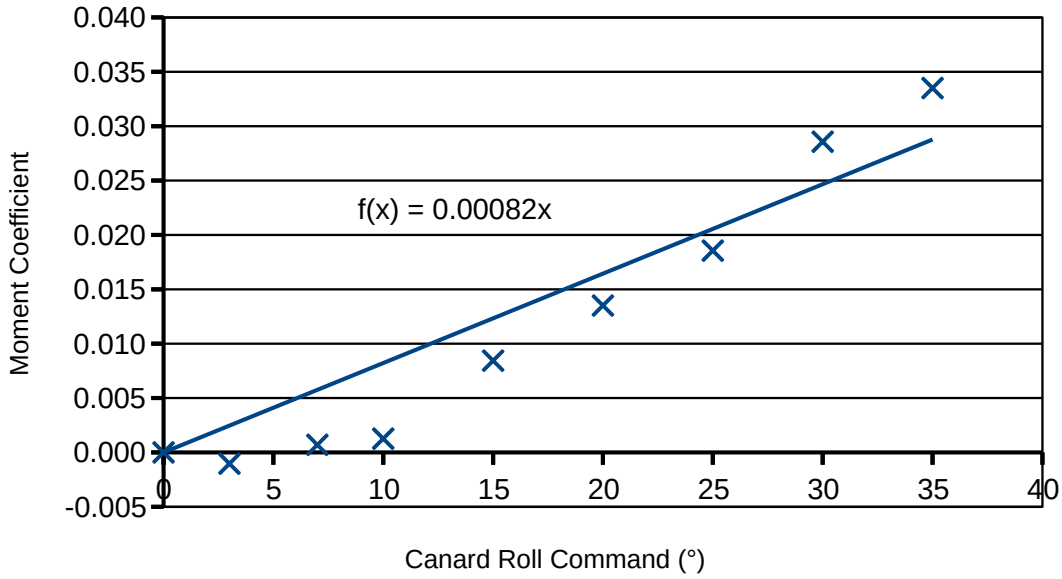


Figure 17: Rolling moment coefficient against canard roll command, gradient is used to calculate the control derivative L_{dp} using reference area, $S = 3 \times 10^{-3} \text{ m}^2$ and reference length, $x = 1 \text{ m}$. The behaviour is clearly non-linear due to the complex coupling between the canards and aft fins (section 4.2), however for a first approximation an approximate linear fit will be used.

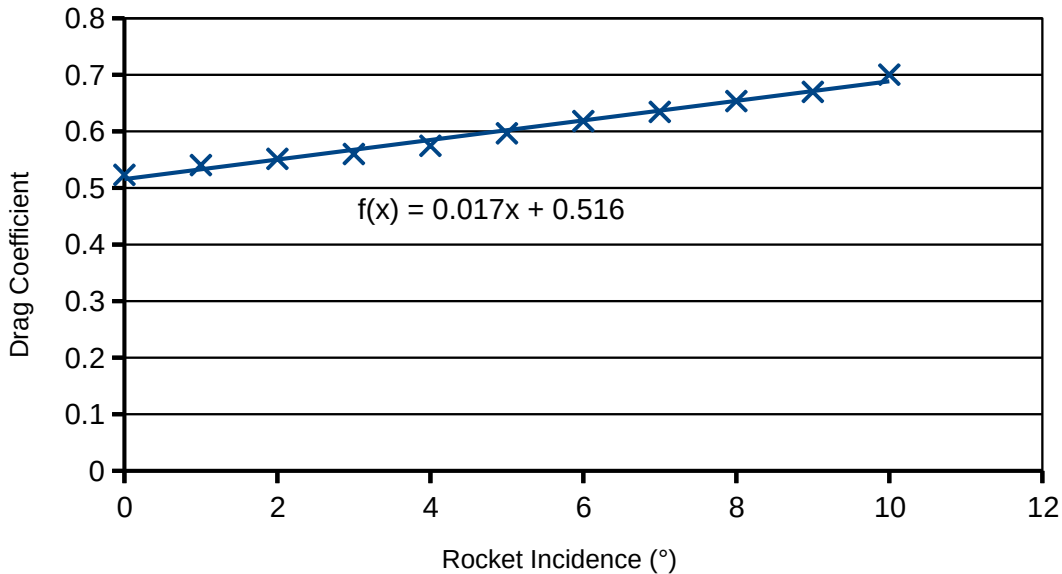


Figure 18: Drag coefficient against incidence, the gradient is used to calculate the control derivative X_u using reference area, $S = 7.85 \times 10^{-3} \text{ m}^2$. The behaviour is clearly linear as assumed by the model. The intersect provides the drag coefficient at zero incidence.

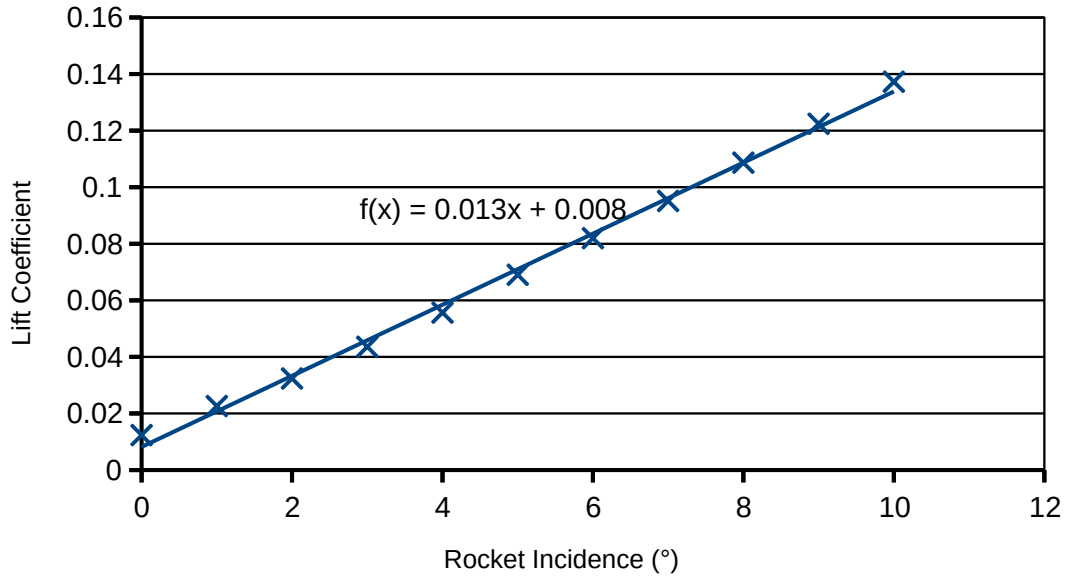


Figure 19: Lift coefficient against incidence, the gradient is used to calculate the control derivative Z_w using reference area, $S = 0.2 \text{ m}^2$. The behaviour is clearly linear as assumed by the model. The non zero intersect is due to a steady state error in the incidence values measured in the wind tunnel.

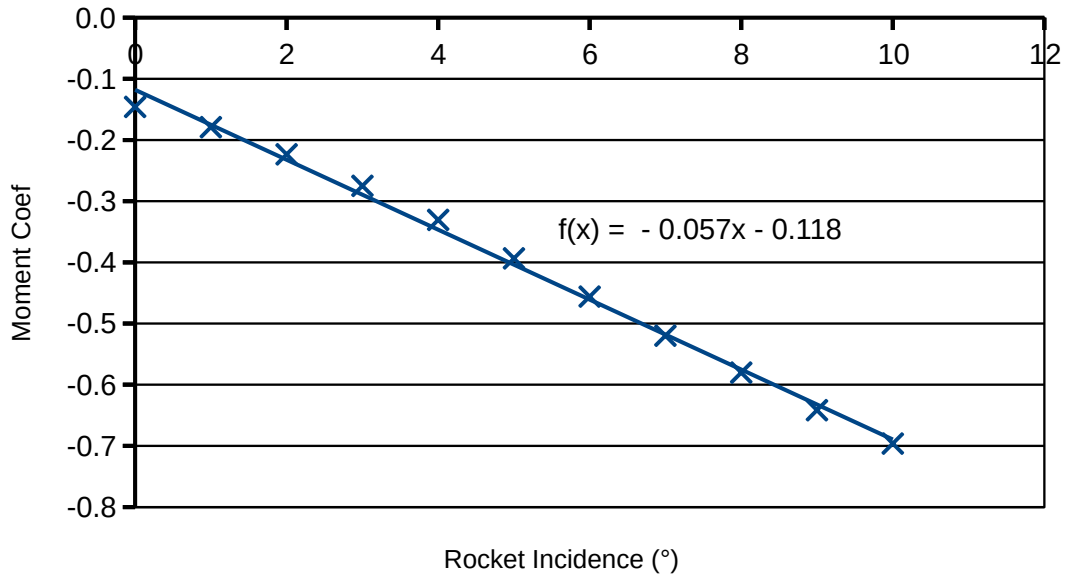


Figure 20: Pitching moment coefficient against incidence, the gradient is used to calculate the control derivative M_w using reference area, $S = 0.01 \text{ m}^2$ and reference length, $x = 1 \text{ m}$. The behaviour is clearly linear as assumed by the model. The non zero intersect is due to a steady state error in the incidence values measured in the wind tunnel.

Stability Derivatives $1/\rho U$			
X_u	-4.08×10^{-3}	L_p	-2.78×10^{-4}
Y_v	-3.7×10^{-3}	M_w	-1.64×10^{-2}
Y_r	4.15×10^{-2}	M_a	-2.74×10^{-2}
Z_w	-3.7×10^{-3}	N_v	1.64×10^{-2}
Z_q	-4.15×10^{-2}	N_r	-2.74×10^{-2}
Control Derivatives $1/\rho U^2$			
Y_{dr}	2.06×10^{-3}	M_{dq}	2.49×10^{-3}
Z_{dq}	2.06×10^{-3}	N_{dr}	2.49×10^{-3}
L_{dp}	7.05×10^{-5}		
Body properties			
m	4.56 kg	I_y	1.31 kg m^{-2}
I_x	$7.9 \times 10^{-3} \text{ kg m}^{-2}$	I_z	1.31 kg m^{-2}

Assuming linearity, the symmetry of the pitch and yaw planes implies that motions in pitch are decoupled from motions in yaw. Furthermore symmetry means pitch and yaw cannot contribute to roll motions and vice versa. The equations of motion then follow from applying Newton's second law. For roll:

$$L_p p + L_{dp} dp = I_x \dot{p} \quad (13)$$

In pitch there are a pair of coupled equations (the yaw equations are of the same form):

$$Z_w w + Z_q q - mg\theta + Z_{dq} dq = (\dot{w} - Uq)m \quad (14)$$

$$M_w w + M_q q + M_{dq} dq = I_y \dot{q} \quad (15)$$

Applying Laplace transforms and writing in matrix form produces the following result.

$$\begin{bmatrix} w \\ \theta \end{bmatrix} = \frac{1}{\Delta} \begin{bmatrix} (M_q - I_y s) & mg - (Z_q + Um)s \\ -M_w & Z_w - ms \end{bmatrix} \begin{bmatrix} -Z_{dq} \\ -M_{dq} \end{bmatrix} dq \quad (16)$$

$$\Delta = mI_y s^3 - mM_qs^2 - Z_w I_y s^2 + (Z_w M_q - M_w(Z_q + Um))s + M_w mg$$

5.2 Roll stabilisation

The transfer function between roll command and roll angle is.

$$\frac{\phi}{dp} = \frac{L_{dp}}{L_p s - I_x s^2} \quad (17)$$

The servo response can be modelled as a first order lag.

$$\frac{dp}{dp_C} = \frac{T_E^{-1}}{s + T_E^{-1}} \quad (18)$$

The servos are rated to move 60° in 0.2s, assuming they move to the nearest degree in this time the resulting time constant T_E is 0.05s. Figure 21 shows the block diagram of a simple proportional controller.

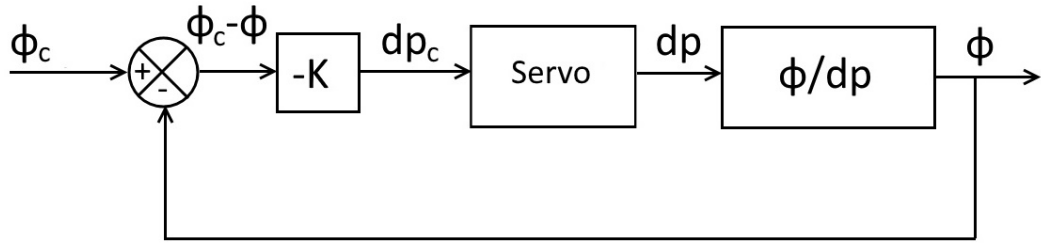


Figure 21: Block diagram of proportional roll angle control, ϕ_c is the commanded roll angle, dp is the canard position and ϕ is the roll angle of the rocket.

The root locus plot with the velocity at 100 ms^{-1} is shown in figure 22, the blue crosses show the locations of the open loop poles, in this case there are no zeros. By selecting the gain (the value of K in the block diagram) the poles of the closed loop transfer function can be placed at the desired location along the paths. The red crosses mark a location with $K=0.05$, this is a good value because the damping ratio here is 0.85 which is sufficiently high to ensuring a well damped response. Figure 23 shows the root locus plot with the velocity at a much lower 20 ms^{-1} . It is clear that the large change in speed has not significantly changed the required gain. For the same gain of 0.05 the damping ratio is slightly higher at 0.92.

Figure 24 shows the effect of the controller on the unit impulse response of the system.

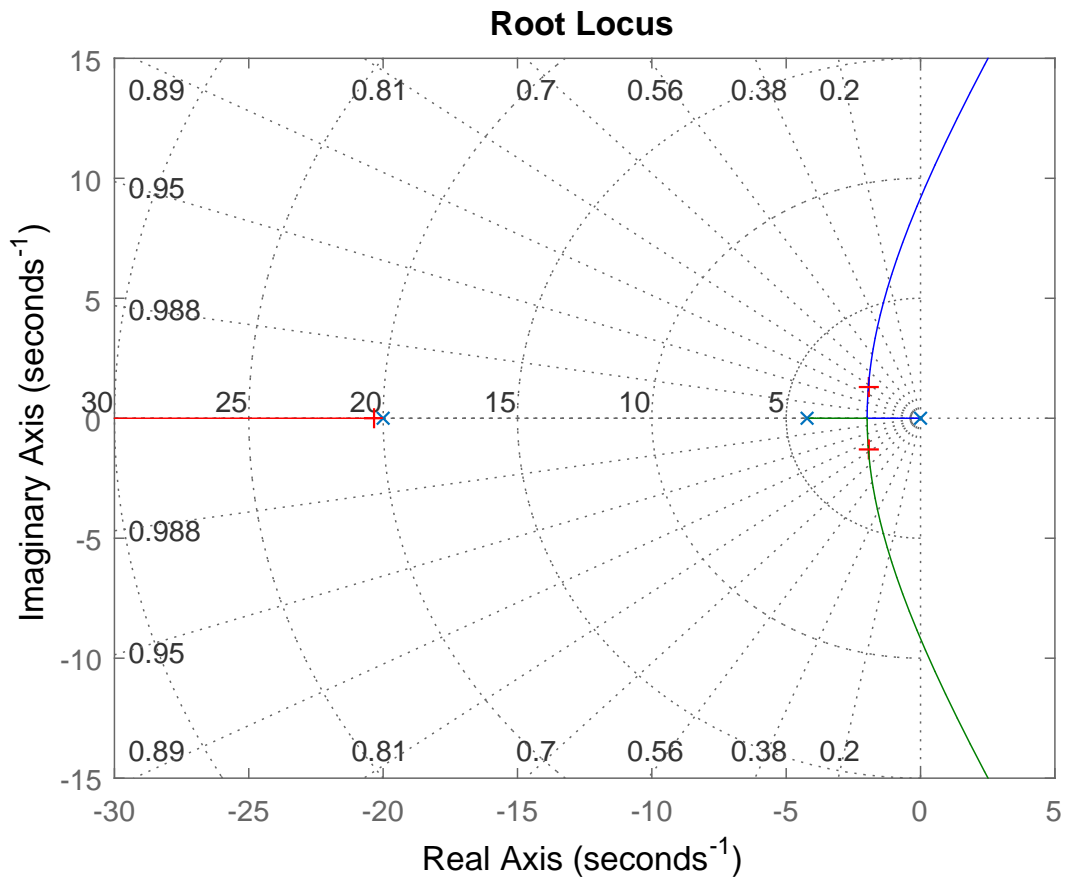


Figure 22: Root locus plot for roll controller for a velocity of 100 m/s. Blue crosses mark the open loop poles, red crosses mark the closed loop poles with a gain of 0.05. Poles in the left hand half plane are stable where as poles in the right hand half plane are unstable, the angle subtended by the pole with the real axis correspond to the damping ratio.

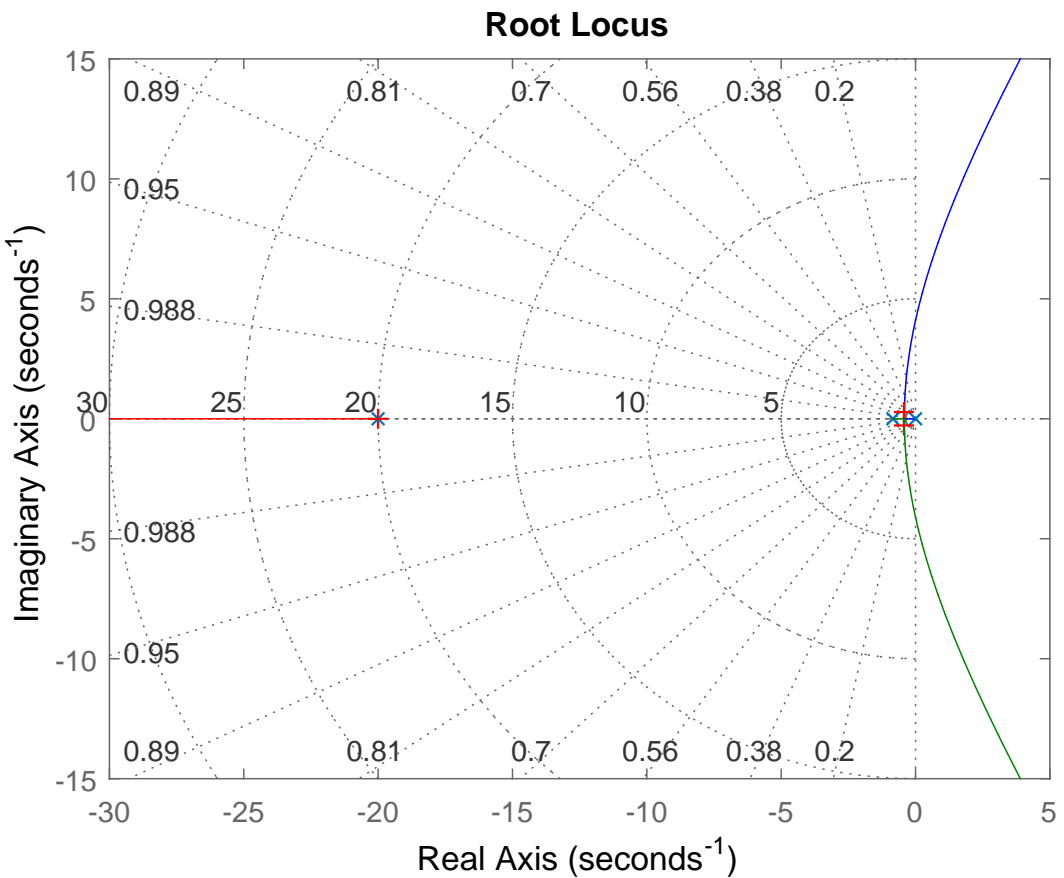


Figure 23: Root locus plot for roll controller same as figure 22 but with $U = 20 \text{ m/s}$. This results in the closed loop poles for the same gain of 0.05 having higher damping.

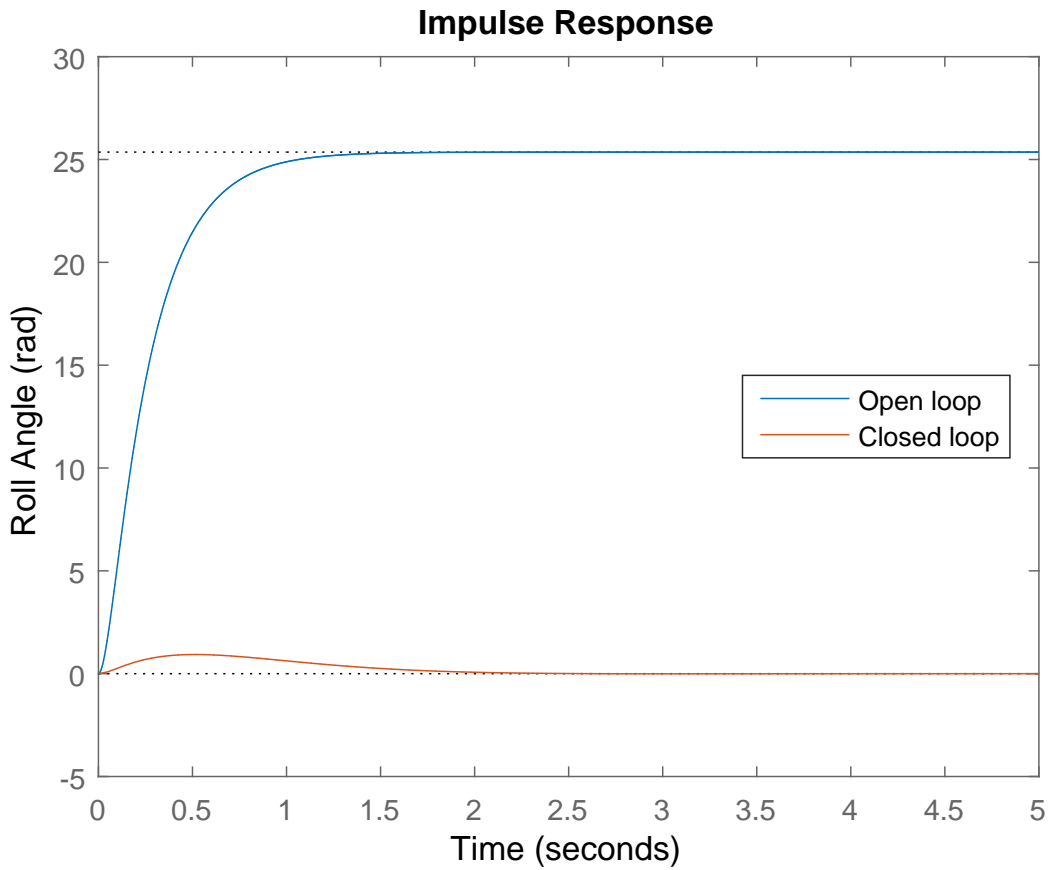


Figure 24: Impulse response of roll controller at $U = 100 \text{ m/s}$ showing the dramatic improvement resulting from the feedback.

Without feedback the rocket could essentially end up at any roll angle. Figure 25 shows the step response of the closed system, a nicely damped response with negligible steady state error.

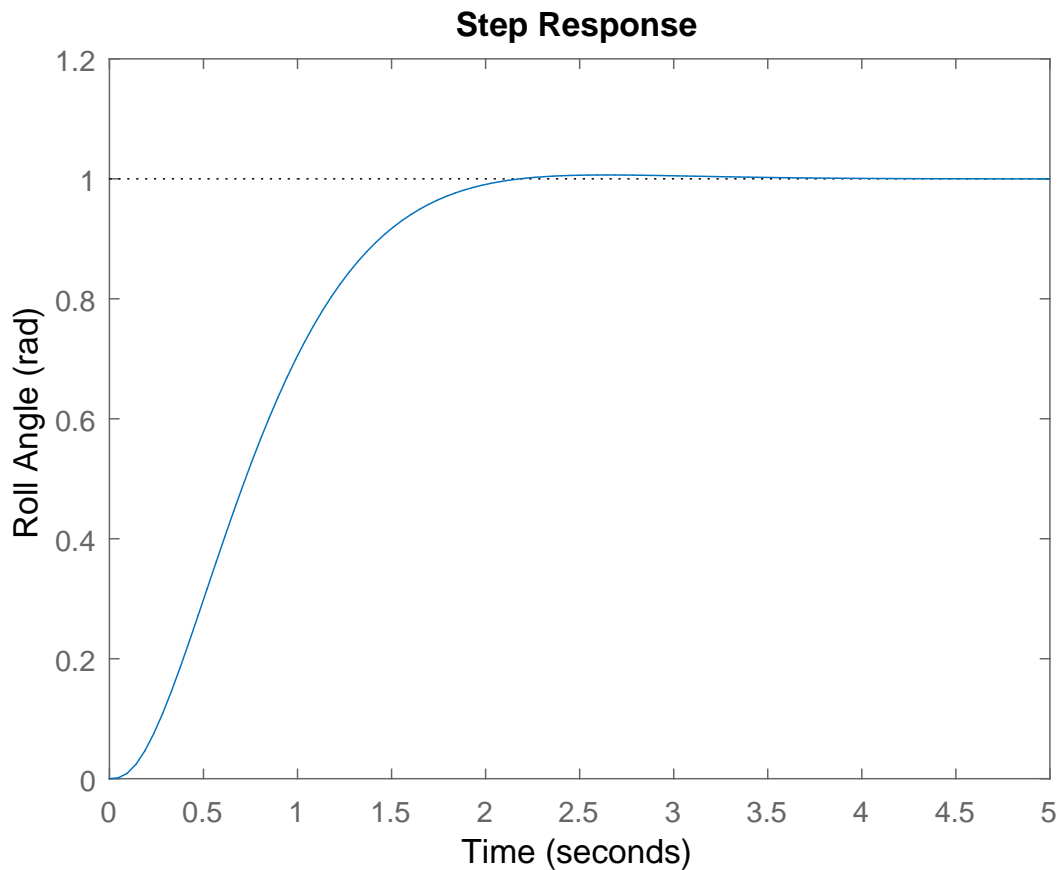


Figure 25: Step response of roll controller at $U = 100 \text{ m/s}$ showing a well damped response with negligible steady state error.

5.3 Pitch and Yaw Autopilot

A similar approach is taken for the pitch and yaw autopilots, which are taken as identical due to symmetry. The transfer function for the pitch command to pitch rate is:

$$\frac{q}{dq} = \frac{mM_{dq}s^2 + (M_wZ_{dq} - Z_wM_{dq})s}{mI_y s^3 - mM_qs^2 - Z_wI_y s^2 + (Z_wM_q - M_w(Z_q + Um))s + M_wmg} \quad (19)$$

The pitch motion is lightly damped therefore in order to implement a useful pitch angle controller the pitch rate response must first be improved. The overall block diagram is shown in figure 26, it consists of an inner pitch rate loop and an outer pitch angle loop with an integrator, which is equivalent to a proportional integral differential (PID) controller on pitch angle. Figure 27 shows the root locus of the pitch rate controller at a speed of 100ms^{-1} , the blue circles are the locations of the zeros. The red crosses show the location with greatest damping ratio (0.37), the gain required is 0.7. Figure 28 shows the improvement in the impulse response with feedback.

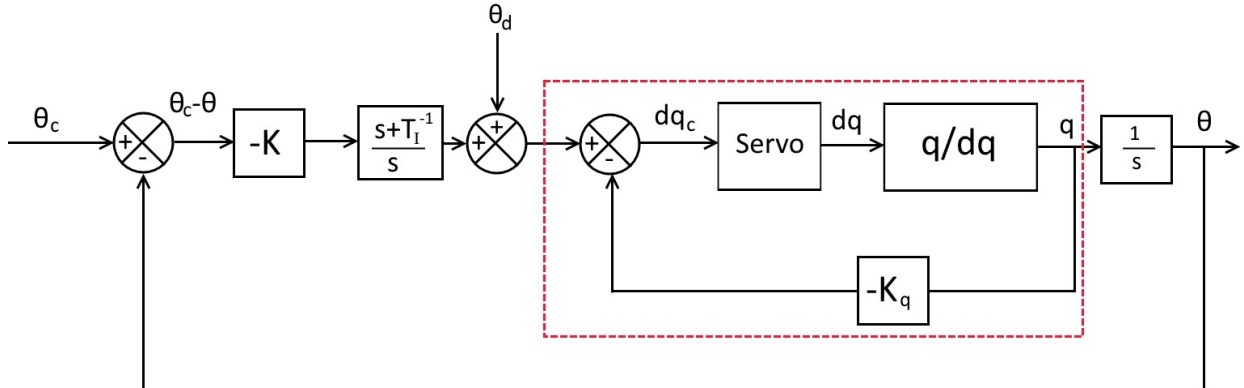


Figure 26: Block diagram of proportional pitch control, showing inner pitch rate loop (red box) and outer pitch angle loop, the integrator is contained in the second box from the left, this provides three constants to tune: K , T_I and K_q . θ_d is a disturbance input.

The inner loop is closed and the response from an impulsive disturbance (θ_d) for the open loop outer system is plotted in figure 29 which shows a steady state error. This is because whilst the rocket is not aligned with the air flow it gains a lateral velocity due to its lift force, this means the angle of zero incidence for the fins is no longer the same as the pitch angle. An example of such an event is weather cocking which can be modelled by an impulse in θ_d , therefore the response should be improved to reduce the effect of weather cocking.

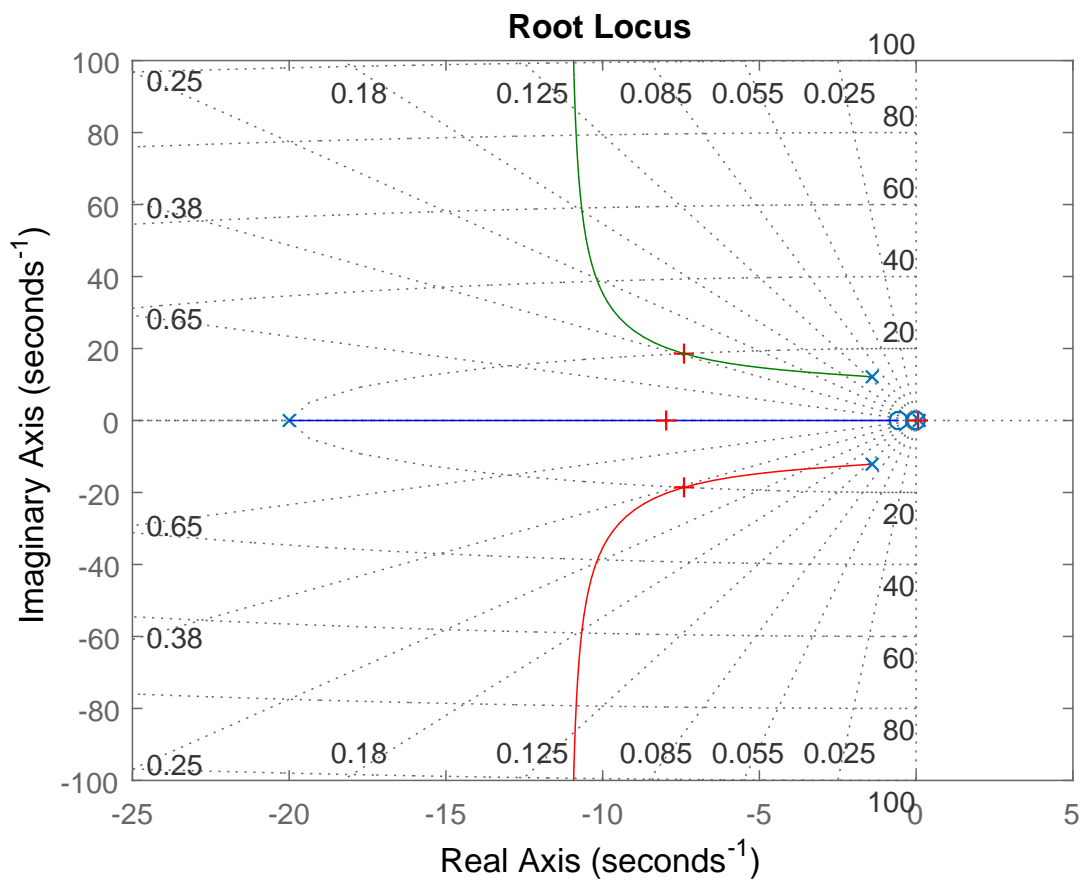


Figure 27: Root locus plot for pitch rate controller for a velocity of 100 m/s. Blue crosses mark the open loop poles, blue circles mark the open loop zeros and the red crosses mark the closed loop poles with a gain (K_q) of 0.7 giving the highest damping ratio of 0.37

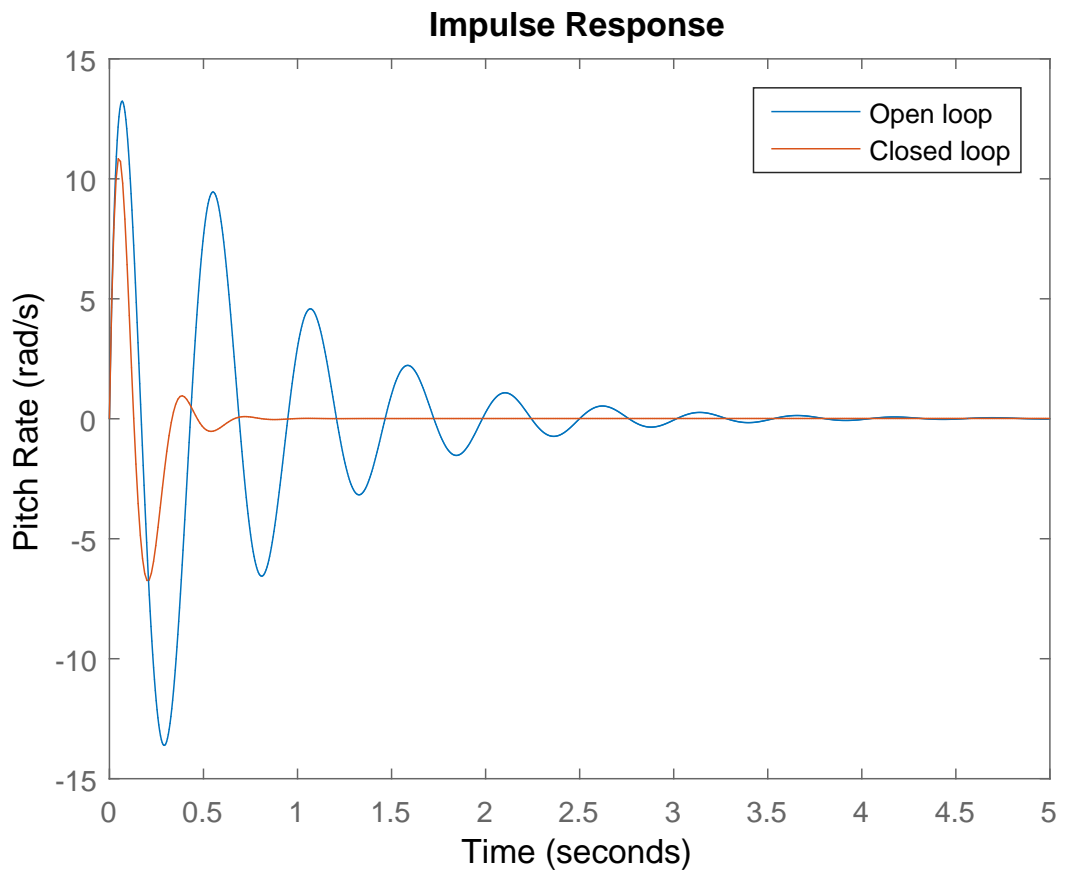


Figure 28: Impulse response of pitch rate controller at $U = 100 \text{ m/s}$ showing a dramatic improvement with feedback however there is still significant overshoot of about 60%.

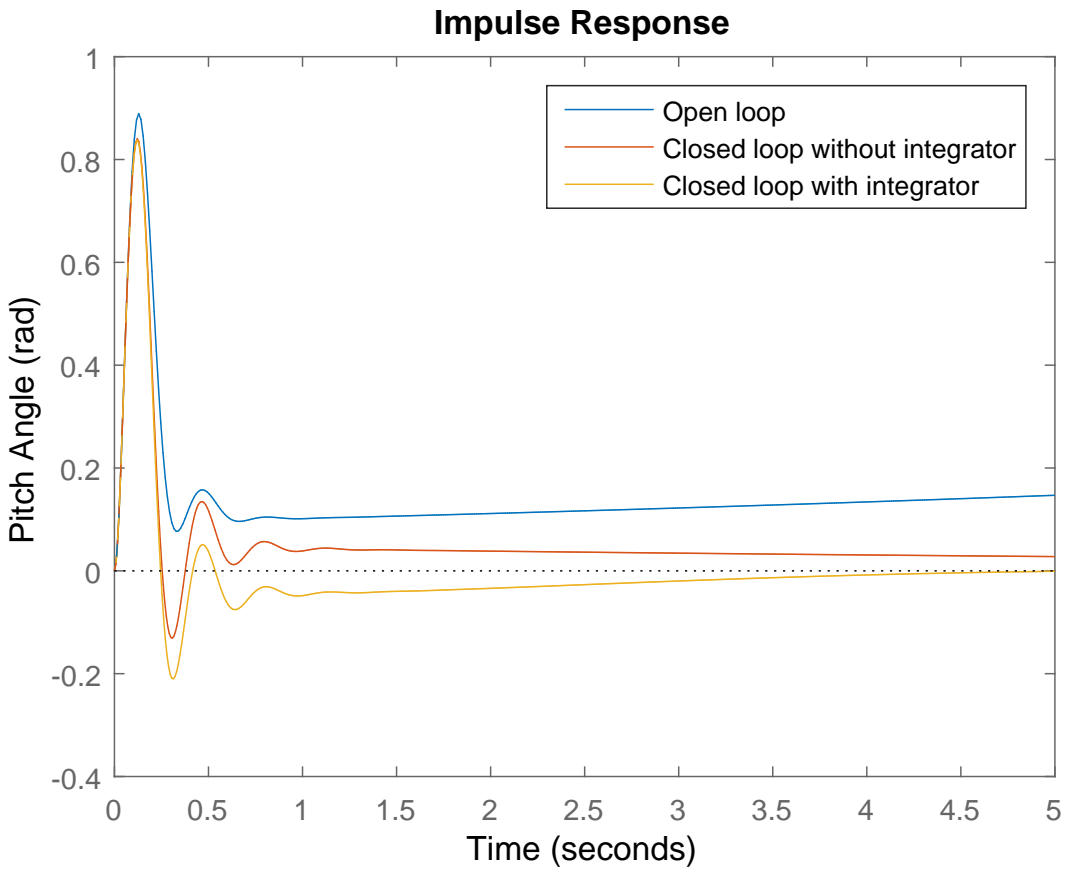


Figure 29: Response from an impulsive disturbance of the pitch angle controller at $U = 100\text{m/s}$ showing: steady state error of open loop response; a proportional controller with a gain of 3 is a significant improvement; and the elimination of steady state error by integral action (again with a gain of 3) at the expense of increased overshoot.

The root locus of the outer loop in figure 30 shows that any increase in gain will reduce the damping ratio leading to a trade off between reducing steady state error and increased oscillation. The resulting step response (figure 31) shows a large steady state error even with a high gain. This can be removed by integral action in the controller. A value for T_I , the integrator time constant must be chosen, the smaller the value of T_I the greater the influence of the integrator. After some trial and error a value of 0.4s has been chosen. The resulting improvement with a gain (K) of 3 is clear in figures 29 and 31.

An investigation into the effect of velocity shows it to be much more important to the pitch response of the rocket compared to the roll response. Fundamentally the aerodynamic forces increase with U^2 whilst the inertial and gravitational forces are constant. Therefore the control system performs better the higher the velocity. The root locus of the pitch rate loop

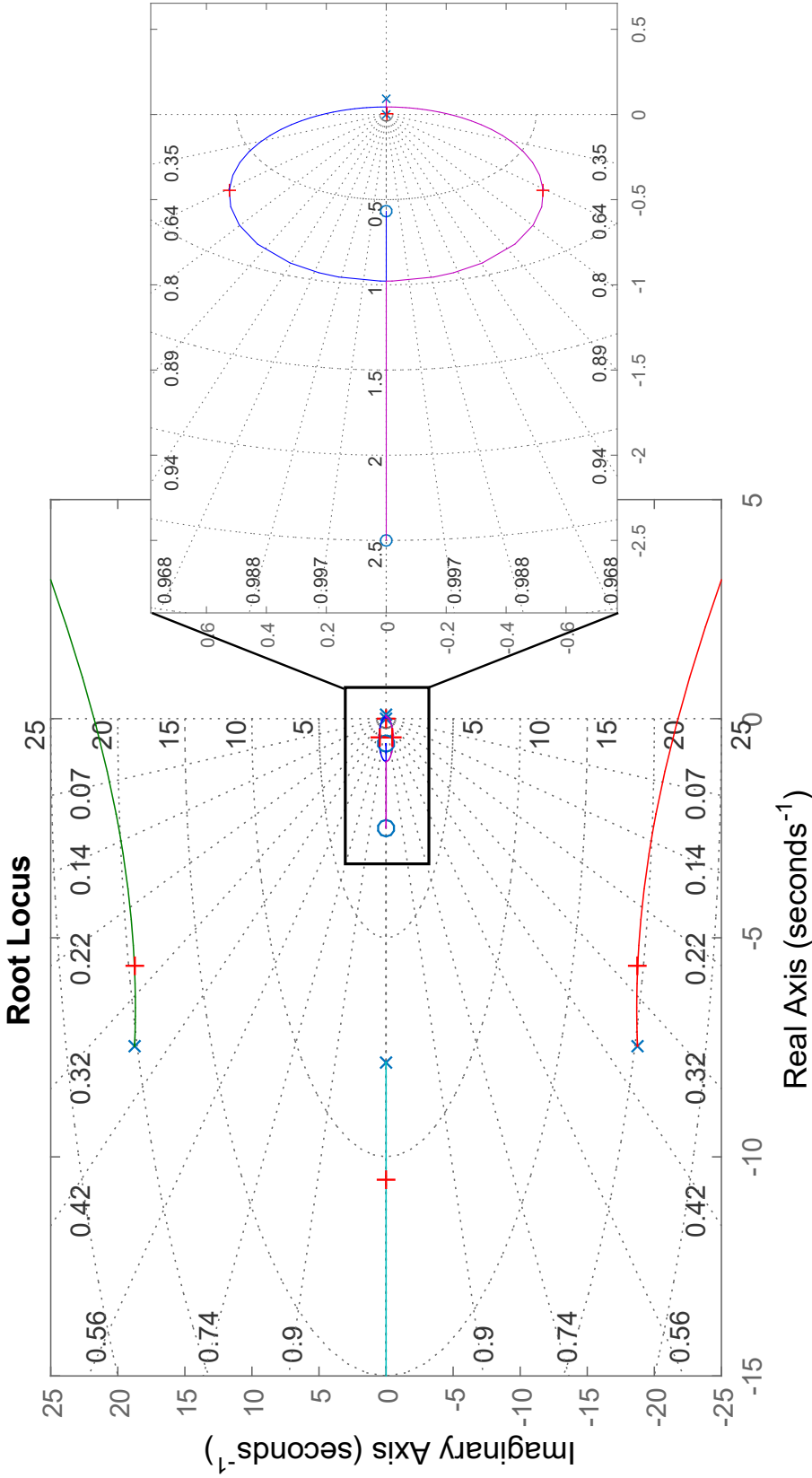


Figure 30: Root locus plot of pitch angle controller for a velocity of 100 m/s, with scale up of the region around the origin. Red crosses mark the closed loop poles with a gain (K) of 2. Increasing gain stabilises the pole near the origin but destabilises the oscillatory mode (blue and green paths) therefore a compromise must be made. The unstable pole in the right hand half plane is due to gravity acting on the rocket, once the pitch angle becomes non zero the rocket's weight will provide a centripetal acceleration causing the rocket's flight path to curve, this is normally a small effect. A high enough gain stabilises this pole.

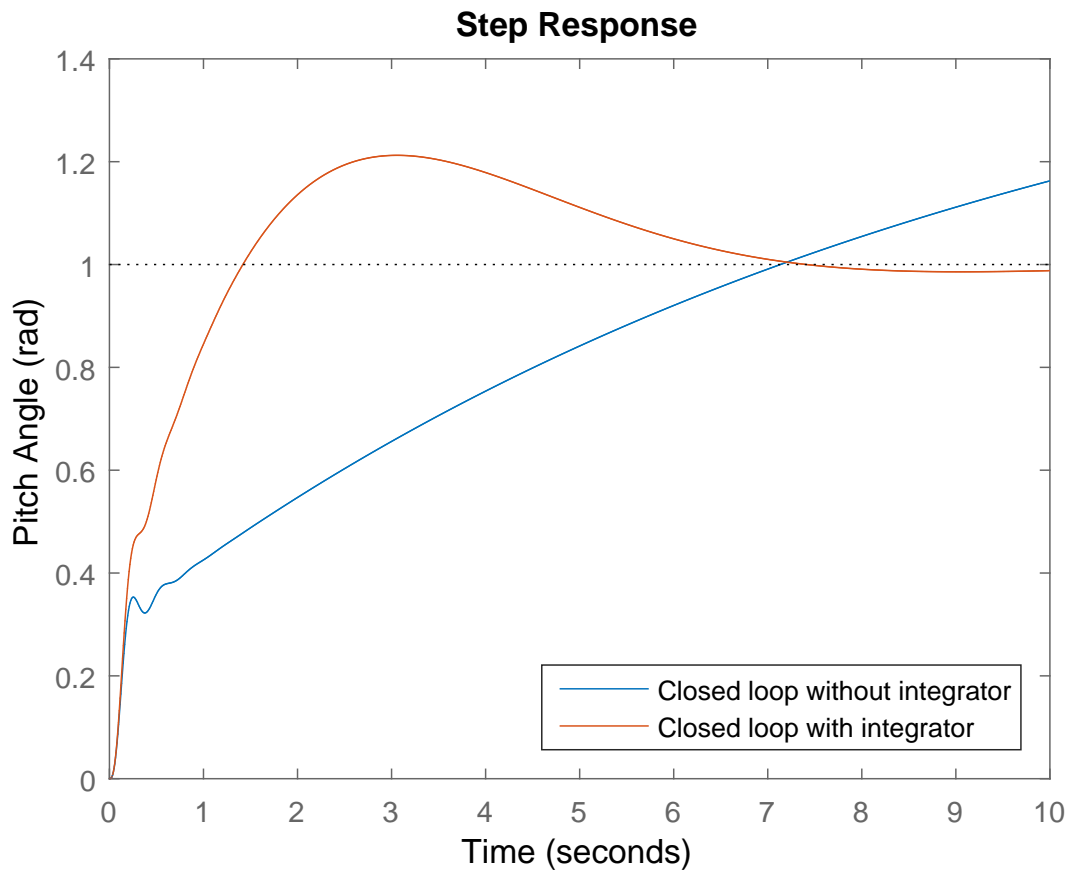


Figure 31: Step response of pitch angle controller at $U = 100 \text{ m/s}$ showing dramatic improvement due to integral action. Gain (K) is 3, integrator time constant (T_I) is 0.4s.

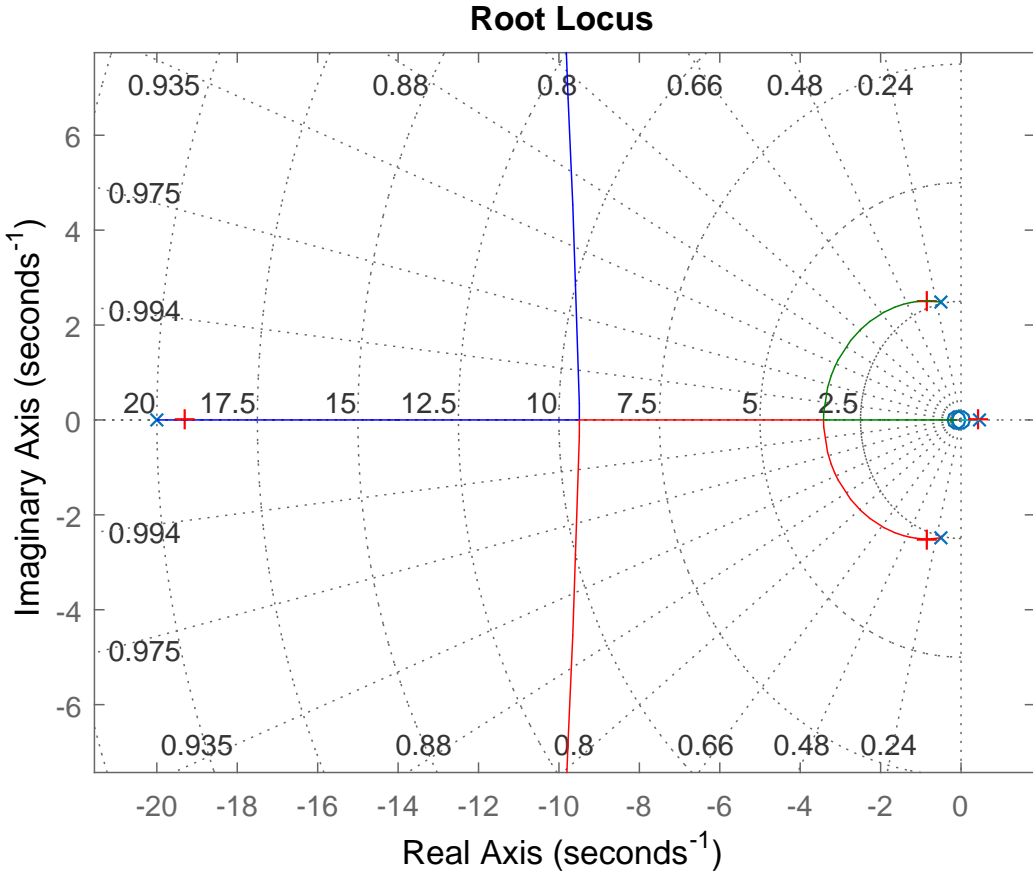


Figure 32: Root locus plot for pitch rate controller for a velocity of 20 m/s. The red crosses mark the closed loop poles with a gain (K_q) of 0.7 giving a damping ratio of 0.31. The character of the plot has completely changed from the one at 100 m/s.

at a velocity of 20 m/s (figure 32) contrast markedly with the one at 100 m/s (figure 27). At the lower speed the gain (K_q) could be much higher. The root locus plot of the pitch angle controller (figure 33) shows that for the gain ($K=3$) used at 100 m/s the system is lighter damped. Therefore the value of K should be chosen to ensure the rocket is not unstable during the low speed sections of flight, alternatively the velocity of the rocket measured by the IMU could be used to update the controller gains on the fly.

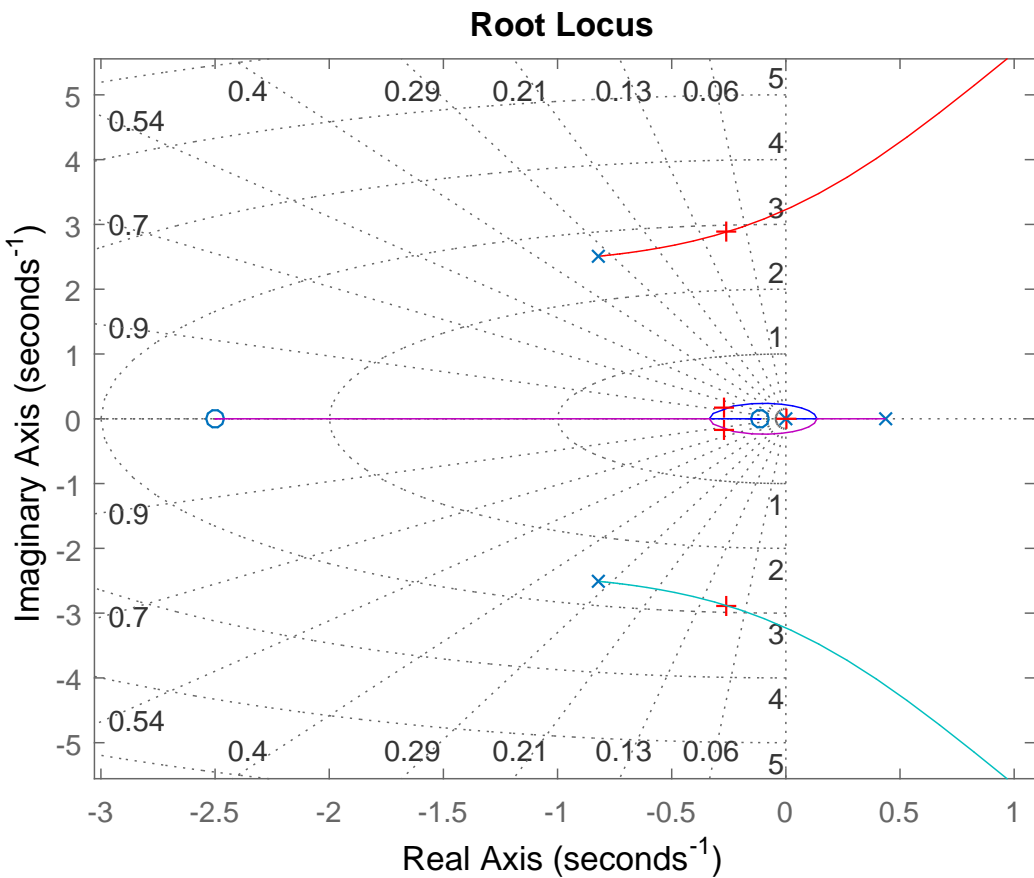


Figure 33: Root locus plot for pitch angle controller for a velocity of 20 m/s. The red crosses mark the closed loop poles with a gain (K) of 3 giving a damping ratio of 0.1.

6 Test Launches

Two launches have taken place, both without canards in order to test the recovery system, both were unsuccessful for different reasons. A flight with canards has not taken place due to difficulty in launching an experimental rocket at UKRA launch sites. However the safety and technical committee have approved the project.

6.1 January

The parachute ejection charges are designed to use approximately 2 grams of black powder (BP) to pressurize the parachute compartment. Black powder was unexpectedly hard to acquire at the launch events and only a substitute called smokeless powder (SP) was available for the first launch. Smokeless powder has been designed as a replacement for BP in firearms applications. However the chemistry of SP is quite different to BP, in particular its reaction rate is far more sensitive to pressure.[9] When used as an ejection charge the powder is far less contained than in the barrel of a gun. After several ground based trials it was found that an aluminium capsule with a rubber burst diaphragm could contain the SP sufficiently for rocket separation (figures 35 and 36).

The rocket made its maiden flight at Midlands Rocketry Club on 10th January (figure 34). The flight up was straight but with some spinning. The rocket separated correctly at apogee however the main did not deploy resulting in a hard landing and some airframe damage. All charges fired but the pressure generated in the main compartment was not sufficient to break the shear pins. This has been attributed to the sensitive nature of SP to how it is contained. Data was collected from the flight, figure 37 shows altitude data and figure 38 shows angular velocity. The angular velocities have been used to compute the attitude of the rocket through the flight based on the principle described in section 3.1. By comparison with on board video this has validated the IMU.

6.2 March

The rocket was repaired and ready for another launch at East Anglian Rocketry Society on 6th March, this time using BP for the ejection charges. Again the ascent was fine but the rocket went through apogee without separating, a flash was noted from the ground. The



Figure 34: The maiden flight took place on 10th January at Midlands Rocketry Club, the rocket is about 10m above the ground and flying straight, photo taken by Andy Mell from UKRA.

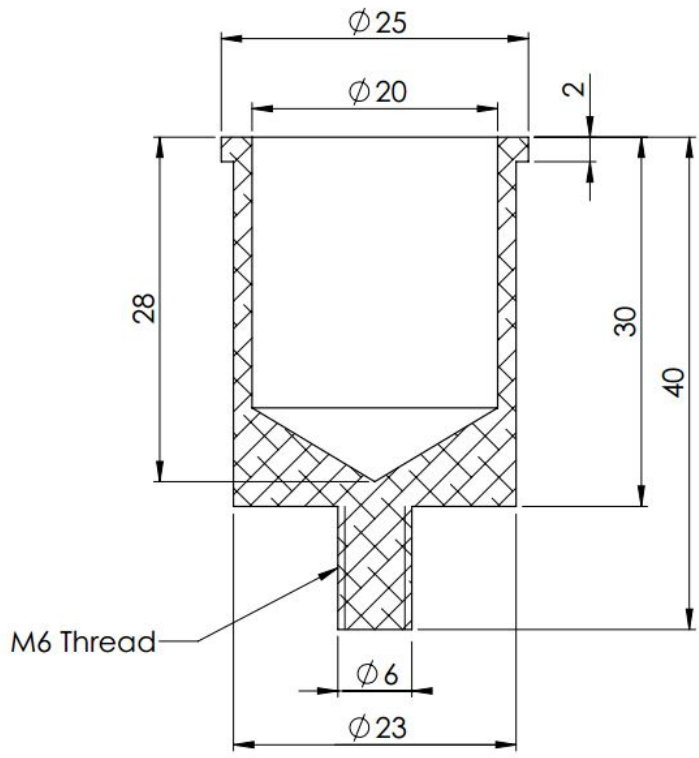


Figure 35: Cross section of aluminium charge holder, dimensions in mm. The thread at the bottom is used to fix it to the bulkhead. The charge is loaded by first positioning an e-match at the bottom of the cup and covering with powder, wadding is then pressed in to keep the powder in contact with the igniter. Finally a burst diaphragm seals the open end.



Figure 36: An ejection charge ready for launch, the holder is mounted to the bulkhead with the e-match connecting via a terminal block to the flight computer on the far side of the bulkhead. Two eye bolts and Kevlar cord form a Y which the shock cord and parachute are attached to.

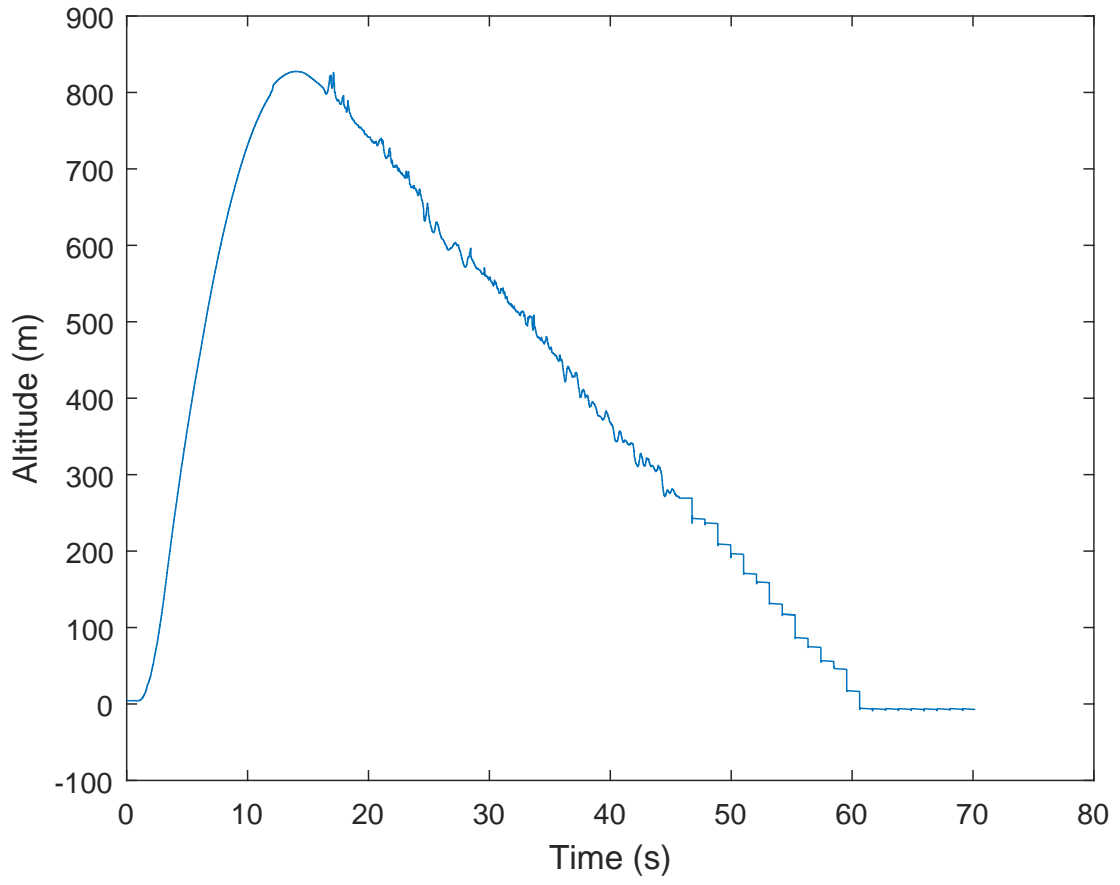


Figure 37: Altitude data from the January launch, showing apogee to be about 825m (Open-Rocket predicted 807m). The noisy descent is a result of the tumbling (the drogue was removed to decrease drift due to high winds), which resulted in a terminal velocity of 18 ms^{-1} .

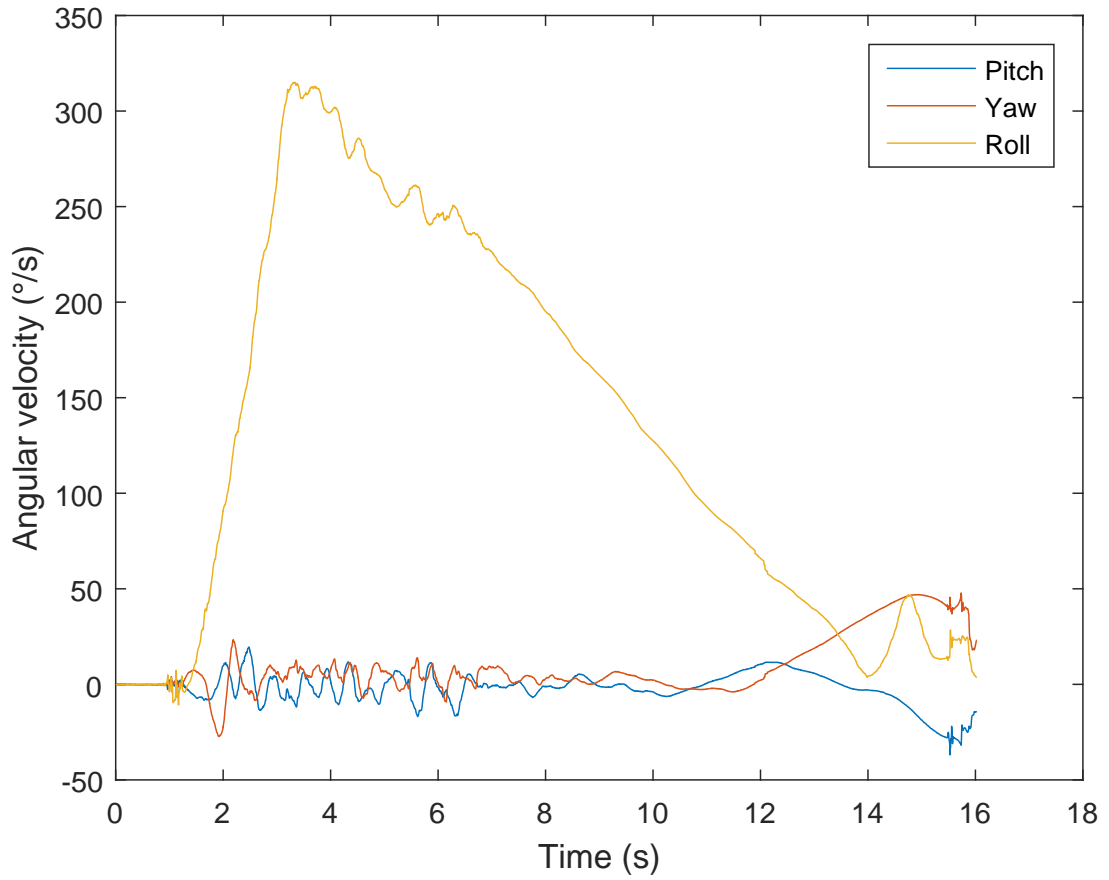


Figure 38: Angular velocity data between launch and apogee from the January launch. The chart shows considerable spinning, reaching a maximum just below 1 revolution per second. The spinning is caused by fin misalignment which explains why the roll rate follows the velocity profile. There is clearly some oscillation during the first 4s of flight. At apogee the rocket loses stability as shown by the last 2s of the graph.

rocket then descended ballistically, thankfully into an empty field. About 30m above the ground the rocket separated and the drogue deployed. The airframe sustained significant damage.

The PerfectFlite computer had failed to fire either charge, despite signalling continuity of both e-matches prior to launch. It appears the capacitor was damaged in the prior crash which explains this failure. The motor ejection charge fired briefly after apogee producing the flash observed. However a new 3D printed altimeter bay was in use which due to a manufacturing defect did not form a sufficient seal between the drogue parachute bay and the vented altimeter bay. This meant the drogue bay did not pressurise enough to break the shear pins.

The second flight computer was programmed to deploy the main at 250m however due to the high velocity of the rocket at this point (likely exceeding 40m/s) the charge fired somewhat lower than this. After separation the main's shock cord went tight due to the sudden increase in drag. This broke the shear pins holding the drogue compartment closed, which then deployed the drogue. This then resulted in high forces from the drogue chute going the other way resulting in the cord failing where it was connected to the FC bay. This was a particular weak point as Kevlar cord was looped around another piece of Kevlar connecting the two eye nuts on the FC bay. A metal ring here would have stopped the Kevlar cutting itself quite so effectively. The tail section then descended under the drogue and was undamaged. The main did not have enough time to deploy, there was about 3 seconds before impact - it was still neatly rolled up on the ground. The hard landing resulting in destruction of the two flight computer bays.

7 Conclusions

To date the project has failed to launch a canard stabilised rocket, however a lot of the work in this direction has been achieved placing this goal well within reach if work continued. In summary a suitable airframe has been built and verified by two test launches, although it now requires some rebuilding of the upper sections. An IMU suitable for the job has been developed and tested confirming the validity of the direct cosine matrix approach to integrating the rate gyroscopes. Furthermore the flight computer has a robust system for deploying a parachute. Perhaps the most interesting part of the project has been the wind tunnel experiments in which naive assumptions that the canards could be modelled as simple

two dimensional flat plates were thoroughly disproved, leading to a greater understanding of the flow around the rocket and providing quantitative data to inform the control system design.

The design of the control system was based on assuming a linear theory, which is at best a rough approximation. Firstly a roll stabilisation system was developed which produced promising results and appears to be only slightly affected by the velocity of the rocket. The pitch autopilot is significantly more complicated due to the coupling between heave velocity and pitch rate. In order to get a reasonable response necessitated a PID controller, which once tuned provided a satisfactory improvement in disturbance rejection (eg. weather cocking). The effect of velocity on the pitch controller is complex and not fully understood, it is clear that a more sophisticated control system could achieve improved performance by changing the control parameters during flight based on speed from the IMU.

Testing has also played a major role in this project requiring a number of problems and failures to be understood and solved. Early launches were delayed and ultimately thwarted by smokeless powder, which has been deemed poorly suited to rocket deployment charges. The importance of rigorously testing recovery systems on the ground has been reinforced by the failures. Ultimately serving as a lesson in the challenges of real life engineering and in particular the unforgiving aspects of rocketry.

The problems with recovery motivate thoughts as to how the system could be improved to be more robust. The use of BP charges is far from ideal, due to: the availability of BP (requiring an explosives licence); fiddly ground testing; hot gasses causing damage to the parachute; and the large number of variables to control. A mechanical system could eliminate these problems at the expense of weight and complexity. The difficulties encountered in the recovery system partly stem from a requirement to use dual deployment. This proved much harder than anticipated and severely hampered development, in retrospect a simpler rocket with a single chute whilst reducing the flight time would have allowed development of the control system to proceed faster.

7.1 Future Work

Given more time the airframe could be repaired for further test flights, the next flight should establish a baseline with the canards in place but not actuated. The roll controller should then be tested to see if roll authority is achieved. It should be evident from the

response whether the system is over or under damped and the size of the steady state error and appropriate adjustments could be made. If this is successful then pitch and yaw control could be included and tested. A full analysis of the canard sizing has not been undertaken, this requires consideration of the maximum disturbances or step changes that will occur. These can be applied to the controller model to determine if the canard command exceeds acceptable values (around 30°). The complex nature of the aerodynamics and control system requires further understanding which could be achieved by more extensive wind tunnel testing. This would be best done using a scale model of the rocket because it would be much easier to test. Factors that could be investigated include: canard size, shape and placement; flow visualisation of canard fin coupling; transient effects; and supersonic flow behaviour.

7.2 Alternative Paths

Testing proved problematic, therefore the design should be focused around easier testing. There is a trade off between smaller rockets which are cheaper and somewhat easier to test but harder to work on and have shorter flight times. However a rocket employing only single deployment is very advantageous. Whilst rocket construction was achieved on schedule at the start of the project problems with BP and poor weather delayed the first launch by several months. The reliance on using UKRA launch sites and the limited availability of BP and rocket motors hindered development. Canards were considered an attractive option at the outlay due to their ability to operate over the duration of the upwards flight compared with thrust vectoring, which is severely limited by the short burn times of solid rocket motors, typically a couple of seconds. The only other sensible alternative is cold gas thrusters whilst being significantly heavier than canards they do offer a number of attractions that were not originally considered. Firstly the torques generated should be much easier to calculate accurately than the aerodynamic forces from the canards. Secondly it would be easier to test in the laboratory without the need for a wind tunnel which are always in demand.

8 References

- [1] *The Rocketry Blog*. URL: <https://rocketry.wordpress.com/2014/08/18/amateur-rocket-team-launches-rocket-to-73-1-miles/> (visited on 05/20/2016).
- [2] *Cesaroni Technology*. URL: <http://www.pro38.com/products/pro54/motor.php> (visited on 11/05/2016).
- [3] Sampo Niskanen. *OpenRocket technical documentation*. May 10, 2013.
- [4] William Premerlani and Paul Bizard. *Direction Cosine Matrix IMU: Theory*. May 17, 2009.
- [5] *Cambridge University Markham Wind Tunnel*. URL: <http://www.ati.org.uk/wp-content/uploads/sites/4/2014/01/Cambridge-University-Markham-Wind-Tunnel.pdf> (visited on 05/20/2016).
- [6] *Downwash Effects on Lift*. NASA. URL: <https://www.grc.nasa.gov/www/k-12/airplane/downwash.html> (visited on 04/26/2016).
- [7] Dietrich Küchemann. *A Simple Method for Calculating the Span and Chordwise Loading on Straight and Swept Wings of any Given Aspect Ratio at Subsonic Speeds*. Aug. 1952. URL: <http://naca.central.cranfield.ac.uk/reports/arc/rm/2935.pdf>.
- [8] Melissa McDanie, Christine Evans, and Dan Lesieurte. *The Effect of Tail Fin Parameters on the Induced Roll of a Canard-Controlled Missile*. July 1, 2010.
- [9] Scott Aleckson. *Going Smokeless!* May 21, 2001. URL: <http://www.alaska.net/~aleckson/rockets/smokless.html> (visited on 04/28/2016).